Thermal Modeling of Flow in the San Diego Aqueduct, California, and Its Relation to Evaporation

GEOLOGICAL SURVEY PROFESSIONAL PAPER 1122

Thermal Modeling of Flow in the San Diego Aqueduct, California, and its Relation to Evaporation

By HARVEY E. JOBSON

GEOLOGICAL SURVEY PROFESSIONAL PAPER 1122

UNITED STATES GOVERNMENT PRINTING OFFICE, WASHINGTON : 1980

UNITED STATES DEPARTMENT OF THE INTERIOR

CECIL D. ANDRUS, *Secretary*

GEOLOGICAL SURVEY

H. William Menard, *Director*

Library of Congress Cataloging in Publication Data

Jobson, Harvey E.
Thermal modeling of flow in the San Diego Aqueduct, California, and its relation to evaporation.

(U.S. Geological Survey professional paper ; 1122)
Bibliography: p. 23-24.
Supt. of Docs. no.: I 19.16:1122
1. San Diego Aqueduct, Calif.–Temperature–Mathematical models. 2. San Diego Aqueduct, Calif.–Evaporation–Mathematical models. I. Title. II. Series: United States. Geological Survey. Professional paper ; 1122.
TC764.J62 628.1'5 79-20943

For sale by the Superintendent of Documents, U.S. Government Printing Office
Washington, D.C. 20402

Stock Number 024-001-03266-0

CONTENTS

ILLUSTRATIONS

TABLES

SYMBOLS

A	= Cross-sectional area of the channel;	R_h	= Hydraulic radius;
A_r	= Surface area of a reservoir;	s	= Time-step number, before which the water temperature is assumed to have been constant;
c	= Specific heat of water at constant pressure;		
C_j	= Coefficient in equation 3;	S_a	= Sun altitude in degrees;
C_v	= Heat storage capacity;	T	= Cross-sectional average water temperature;
d_j	= Coefficient in equation 3;	t	= Time;
DT	= Time step;	T_a	= Air temperature;
D_x	= Longitudinal dispersion coefficient;	T_b	= Arbitrary reference temperature;
DX	= Length, in meters of the subreach (1,299 m);	T_i	= Initial temperature of a water parcel as it enters the system;
E	= Rate of evaporation;		
e_a	= Vapor pressure of air;	T_o	= Final temperature of a water parcel as it passes the downstream end of the channel;
e_{jk}	= Coefficient in equation 3;		
e_o	= Saturation vapor pressure of air evaluated at a temperature equal to that of the water surface;	T_w	= Wet-bulb air temperature;
		U	= Cross-sectional average velocity;
$H(t)$	= Increase in heat content of the slab between time zero and t resulting from a unit increase in surface temperature at time zero;	U_*	= Shear velocity;
		V	= Wind speed;
		Vj	= Volume of water in subreach j;
H_b	= Heat flux leaving the water caused by longwave radiation being emitted by the water;	W	= Top width of the channel;
		x	= Longitudinal coordinate;
H_e	= Heat flux leaving the water as a result of the latent heat of vaporization;	y	= Distance above the insulated bottom of the slab at which temperature ΔT_B is computed;
H_h	= Heat flux conducted from the water to the air as sensible heat;	Y_j	= Centerline water depth in subreach j;
		$YM(k)$	= Recorded centerline water depth at recorder k;
H_N	= Net flux to the water caused by incoming radiation from the sun and the sky;	Z	= Thickness of the bed slab;
		α	= Constant in wind function;
H_p	= Flux of thermal energy from the bed to water;	γ	= Psychrometric constant;
H_R	= Heat flux added to the water by rain falling directly on its surface;	$\Delta H(i)$	= Heat flux to the water from the bed during any time step iDT to $(i+1)DT$ to result from a unit increase in water temperature at time zero;
H_T	= Rate of absorption of thermal energy at the water surface per unit area;	ΔT_B	= Temperature rise within the slab;
i	= Rainfall rate;	$\Delta T(jDT)$	= Change in water temperature to occur at jDT;
k	= Thermal diffusivity;	$\Delta\theta$	= Difference between the virtual temperature of the air and the water surface;
L	= Latent heat of vaporization of water;		
N	= Empirical mass-transfer coefficient in the wind function;	ϵ	= Emissivity of water;
		ρ	= Density of water;
P_a	= Atmospheric pressure;	σ	= Stefan-Boltzman constant for black-body radiation;
$Q(j)$	= Discharge at cross-section j;	τ	= Travel time required for a parcel to flow through the system; and
QD	= Diversion discharge;		
r	= Coefficient of correlation;	ψ	= Empirical wind function.
R	= Reflectivity;		

CONVERSION TABLE

Factors for converting metric units to inch-pound units are shown to four significant figures.

Multiply metric unit	*By*	*To obtain inch-pound unit*
meter (m)	3.281	foot (ft)
kilometer (km)	0.6214	mile (mi)
centimeter (cm)	0.03281	foot (ft)
millimeter (mm)	0.3937	inch (in)
meter per second (m/s)	3.281	foot per second (ft/s)
cubic meter per second (m^3/s)	0.02832	cubic foot per second (ft^3/s)
kilopascal (kPa)	10.00	millibar (mb)

THERMAL MODELING OF FLOW IN THE SAN DIEGO AQUEDUCT, CALIFORNIA, AND ITS RELATION TO EVAPORATION

By HARVEY E. JOBSON

ABSTRACT

The thermal balance of the 26-kilometer-long concrete-lined San Diego Aqueduct, a canal in southern California, was studied to determine the coefficients in a Dalton type evaporation formula. Meterologic and hydraulic variables, as well as water temperature, were monitored continously for a 1-year period.

A thermal model was calibrated by use of data obtained during a 28-day period to determine the coefficients which best described the thermal balance of the canal. The coefficients applicable to the San Diego Aqueduct are similar to those commonly obtained from lake evaporation studies except that a greater evaporation at low windspeeds is indicated.

The model was verified by use of data obtained during 113 days (excluding the calibration data). These data verified that the derived wind function realistically represents the canal evaporation. An annual evaporation of 2.08 meter was computed; this amount is about 91 percent of the amount of water evaporated annually from nearby class A evaporation pans.

INTRODUCTION

Because of its large influence on many facets of the ecosystem, water temperature is clearly an important water-quality parameter. The rates of most chemical and biological reactions are temperature dependent, as are the spawning and growth cycles of most fish. The accuracy of any water-quality model is, therefore, sensitive to the accuracy of the thermal model upon which it must depend. The accuracy of a temperature model, likewise, is very dependent on the accuracy of the estimated exchange of energy between air and water. Finally, evaporation is a major component of the surface exchange process. Evaporation is, therefore, a key element in any water-quality model in addition to being a troublesome factor in computing the water balance of a river system.

While evaporation from lakes and reservoirs has received considerable attention, there has been almost no quantitative evaporation measurements from open channels. The purpose of this study and report is to develop a thermal model for open channels and to determine the applicable coefficients for a Dalton-type evaporation formula.

Dalton's law is often expressed as

$$E=\psi(e_o-e_a) \tag{1}$$

in which E=rate of evaporation in units of length per time; ψ=an empirical coefficient or wind function; e_o=saturation vapor pressure of air evaluated at a temperature equal to that of the water surface; and e_a=vapor pressure of the air. For the purposes of this report, the wind function is assumed to have the form

$$\psi=\alpha+NV \tag{2}$$

in which V=windspeed and intercept, α, as well as the mass-transfer coefficient, N, are assumed to be constant for the canal.

The evaluation of the coefficients α and N is difficult for open channels. Southern California offers an excellent average climate for the study of the coefficients in the wind function because the sensitivity of surface exchange to windspeed is large in this area of low humidity and high natural water temperatures. The San Diego Aqueduct, operated by the Metropolitan Water District of southern California, was chosen for determination of these coefficients as it has a relatively shallow depth, usually steady flow, and a simple hydraulic regime as well as being located in a hot, dry climate.

Meterologic data including incoming solar radiation, incoming atmospheric radiation, windspeed, wind direction, air temperature, wet-bulb air temperature, and rainfall were recorded at each end of the canal for a 1-year period beginning July 25, 1973. In addition, the water temperature at each end, the depth at five locations, and the rates of flow at the canal inlet and diversions were monitored. All these data have been presented previously (Jobson and Sturrock, 1976).

The interpretation of these data is accomplished by the use of a one-dimensional, finite-difference, thermal-balance model. The model, which uses both the Eulerian and Lagrangian reference frames, predicts the temperature at the lower end of the canal as a function of (1) the upstream temperature, (2) the rate of surface exchange due to radiation, rainfall, evaporation, and conduction to the air, (3) the exchange of energy between the bed and the water, and

(4) longitudinal mixing within the channel. The contribution of each surface exchange and mixing process to the predicted temperatures is tabulated by use of a model written in the Lagrangian reference frame. This tabulation allows the coefficients in the wind function to be ascertained.

Data collected during 141 days were complete enough for use in calibrating or verifying the thermal model. These 141 days existed in eight groups of continuous data. Every month except January, February, September, and October were represented in the data sets.

The model was developed and calibrated using data obtained during the first 28 days of the study. Calibration in the sense used here implies the determination of the two coefficients in the wind function (eq. 2) which allow the model to best describe the thermal regime of the canal. The model, with the two derived coefficients, was then verified using the remaining 113 days of data. The wind function coefficients found to apply to the San Diego Aqueduct are similar to the values obtained from lake-evaporation studies except that a larger evaporation at zero windspeed is indicated.

The following sections describe the flow and temperature models and the model calibration, including a discussion of a sensitivity analysis. The model verification is then presented. The report is concluded by presenting an estimate of the total evaporation from the canal throughout the year.

MODEL DEVELOPMENT

The temperature in an open channel is dependent on both hydraulic and meterologic variables. The flow, on the other hand, can usually be assumed to be independent of water temperature unless thermal stratification is significant. Flow in the San Diego Aqueduct was modeled independently of the temperature, and a data set was written for each time step which contained the average centerline water depth in each subreach and the discharge at each grid point. This data set was then used as input to the temperature model.

THE FLOW MODEL

The San Diego Aqueduct is a concrete-lined open canal originating near Hemet, Calif., about 120 km southwest of Los Angeles and flowing generally south for about 26 km (see fig. 1) on a slope of 0.00012. The canal's trapezoidal shape has a 3.66 m bottom width and side slopes of 1.5 to 1. At full capacity it delivers about 28 m^3/s, but generally it flows near half capacity. During the study the flow varied from 7 to 24

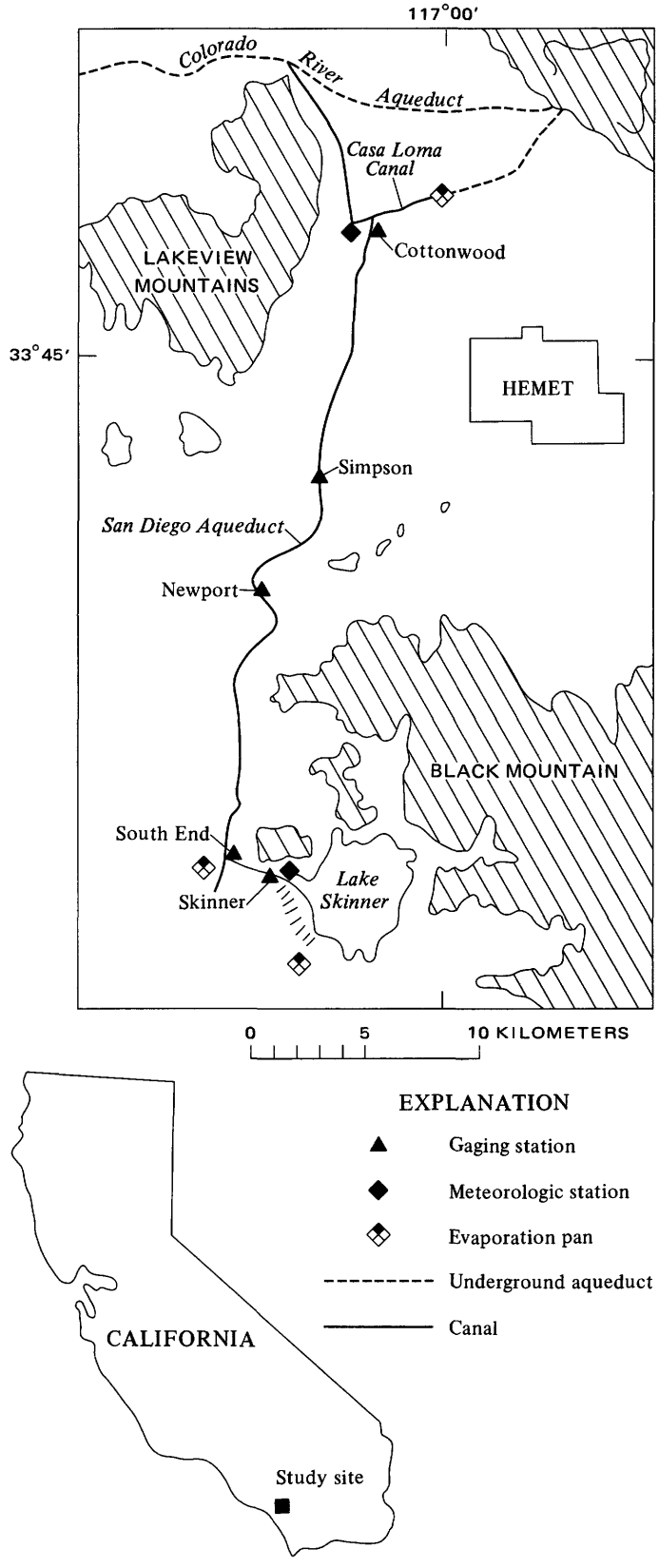

FIGURE 1.—San Diego Aqueduct showing data-collection points.

m^3/s. The maximum design depth is 3.05 m with a 0.305 m freeboard.

The operation of the canal is such that the flow remains steady for several days in a row. Changes usually occur in steps. Because of equipment failures, shutdowns for canal maintenance, and so forth, only 141 of the 365 days were modeled. Changes in discharge ranging from 12 to 60 percent occurred on only 5 days of the 141 days.

Although the flow in the canal was generally steady, it was not uniform. Either the channel roughness or the bottom slope varied slightly with distance along the canal. To account for the nonuniformity of the flow between the five water level recorders (see fig. 1), longitudinal profiles of the centerline depth were measured under five different steady flow conditions. For computational purposes, the canal was schematized into 20 subreaches of equal length. Each subreach and the cross section at its upstream end were represented by the index j. The mean depth in each subreach was determined for each flow. An analysis of these observed depths indicated that the following expression could be used to determine the centerline water depth in each of the 20 subreaches.

$$Y_j = C_j + d_j \sqrt{\frac{YM(4) - YM(3)}{Q(21)}} + \sum_{k=1}^{5} e_{j,k}\, YM(k) \quad (3)$$

in which Y_j=centerline water depth, in meters, for subreach j (j=1, 2, . . . 20 with j=1 at the upstream end); C_j, d_j, and $e_{j,k}$ are constants shown in table 1; $YM(k)$=recorded stage, in meters, at gaging station k, (k=1, 2, 3, 4, 5 with k=1 for the gaging station in the farthest upstream; and $Q(21)$=discharge at the downstream end of the canal, in cubic meters per second. The constant $e_{j,k}$ interpolates the depth from the two nearest gaging stations in proportion to the distance from each station. The term involving d_j accounts for backwater effects and the constant C_j accounts for any vertical displacement of the bed in the subreach. The standard error of estimate for equation 3, among the five flow conditions, ranged from a low of 0.004 m for subreach 12 to a high of 0.069 m for subreach 14. The median value for all subreaches was 0.031 m.

The water volume in each subreach was computed from

$$V_j = (3.658 + 1.5Y_j)\, Y_j DX \quad (4)$$

in which V_j = volume of water in subreach j, in cubic meters; Y_j = mean centerline water depth in meters (from equation 1); and DX = length, in meters, of the subreach (1,299 m). The discharge at each cross section was then computed from the discharge into or out of the canal and continuity using the expression

$$Q(j) = Q(j+1) + QD(j) + [V(j, i+\tfrac{1}{2}) - V(j, i-\tfrac{1}{2})]/DT \quad (5)$$

in which $Q(j)$=discharge at cross-section (j) and time iDT, $V(j, i-\frac{1}{2})$=volume of water in subreach j at time $(i-\frac{1}{2})\,DT$; DT=time step (1 hour used in flow model); and $QD(j)$=discharge diverted from subreach j during the time step. Three diversion points exist. Diversions near Simpson and the South End (fig. 1) were seldom used, and the third, downstream of Newport, is insignificant in size. The volume at time step $i+\frac{1}{2}$ was determined from the average of the depth determined at time step i and time step $i+1$.

TABLE 1.—*Coefficients for use in equation 3 to determine the centerline depth in the San Diego Aqueduct*

[All depths are expressed in meters. The value of d_j is assumed zero if the absolute difference $YM(4) - YM(3)$ is less than 0.04 m and the sign of d_j is negative if $YM(4) - YM(3)$ is negative]

Subreach (j)	C_j	d_j	e_{jk}				
			k = 1	k = 2	k = 3	k = 4	k = 5
1	−0.029	0	1.0	0	0	0	0
2	− .055	0	.841	0.159	0	0	0
3	− .047	0	.689	.311	0	0	0
4	− .052	0	.537	.463	0	0	0
5	− .028	0	.385	.615	0	0	0
6	− .021	0	.235	.765	0	0	0
7	+ .024	0	.081	.919	0	0	0
8	+ .008	0	0	1.0	0	0	0
9	+ .182	0	0	.559	0.441	0	0
10	+ .150	0	0	.259	.741	0	0
11	+ .139	0	0	0	1.0	0	0
12	− .019	0.074	0	0	.872	0.128	0
13	+ .144	.428	0	0	.759	.241	0
14	+ .294	.507	0	0	.646	.354	0
15	+ .226	.519	0	0	.533	.467	0
16	+ .202	.606	0	0	.420	.580	0
17	+ .078	.492	0	0	.308	.692	0
18	+ .125	.399	0	0	.195	.805	0
19	+ .070	.158	0	0	.082	.918	0
20	0	0	0	0	0	.500	0.500

THE EULERIAN TEMPERATURE MODEL

Applying the principle of conservation of thermal energy to a one-dimensional open channel, the governing equation becomes

$$\frac{\partial T}{\partial t} + U\frac{\partial T}{\partial x} = D_x \frac{\partial^2 T}{\partial x^2} + \frac{H_T W}{Ac\rho} + \frac{H_p}{R_h c\rho} \quad (6)$$

in which T=cross-sectional average water temperature; t=time; U=cross-sectional average velocity;

x=longitudinal coordinate; D_x=longitudinal dispersion coefficient; H_T=rate of absorption of thermal energy at the water surface, per unit area; W=top width of the channel; A=cross-sectional area of the channel; c=specific heat of water at constant pressure; ρ=density of water; Hp=rate at which the water absorbs heat from the bed, per unit area; and R_h=hyraulic radius. It is usually found that the cross-sectional temperature variation is small for natural channels (Dingman and Weeks, 1970; Jones, 1965; and Rawson, 1970). Water temperatures were measured at four points in the vertical in the San Diego Aqueduct and vertical stratification was never observed. The specific heat and density are assumed to be constant, and the product of the dispersion coefficient and the area is assumed to be independent of x. All other varialbes, U, W, H_T, A, H_p, and R_h, can be functions of both x and t.

Equation 6 is an Eulerian expression; it is a description of the variation of temperature with respect to a fixed coordinate system. This equation was solved numerically by the finite-difference technique using an implicit six-point forward difference scheme. The method of Stone and Brian (1963) was modified by giving the spatial derivative evaluated at the new time step a weight of 0.55 and the derivative evaluated at the old time step a weight of 0.45. This modification is similar to the method proposed by Fread (1974) for a four-point scheme. A 20-minute time step was selected for use in the temperature model because it was an even multiple of the data recording frequency (10 minutes) and because of economic reasons. Once the time step was determined, the distance step was selected such that the average value of $U\ DT/DX$ was about 1.0 in order to optimize the accuracy of the numerical scheme. Using the same cross sections as in the flow model, the canal length was divided into 20 subreaches (21 grid points).

The last two terms in equation 6 were evaluated by use of meterologic and hydraulic data; the data were evaluated at a time midway between the time steps. If the water temperature is required in evaluating these terms, however, the old value at the cross section was used. It can be easily demonstrated, by use of numerical experiments, that use of the old temperature values has little effect on the accuracy of the solution provided $DT\ W/A\ [\partial(H_T/c\rho)/\partial T] < 0.2$. For a water depth greater than 50 cm, this restriction reduced to $\partial(H_T/c\rho)/\partial T \leq 700$ cm/day. Jobson (1973) has shown that this criteria will be met except under very exceptional conditions. The value of $\partial(H_T/c\rho)/\partial T$ will be recognized as the kinematic surface exchange coefficient.

The next to the last term in equation 6 represents the rate at which the water absorbs energy from the atmosphere. The San Diego Aqueduct contains several inverted siphons to carry the water under roadways or drainageways. When a subreach contained a siphon the effective surface area of the subreach was reduced to account for the fact that no surface exchange can occur unless there is a free surface. Siphons were assumed to have no effect on the velocity or volume of water in the subreach.

For purposes of this report, the surface exchange will be expressed as the sum

$$H_T=H_N-H_b+H_R-H_e-H_h \tag{7}$$

in which H_N=net heat flux to the water caused by incoming radiation from the sun and the sky; H_b=heat flux leaving the water caused by longwave radiation being emitted by the water; H_R=heat flux added to the water by rain falling directly on its surface; H_e=heat flux leaving the water as a result of the latent heat of vaporization of the evaporated water; and H_h=heat flux conducted from the water to the air as sensible heat.

The net incoming radiation is composed of four components: The solar radiation incident to the water surface less the reflected component plus the incoming atmospheric radiation less its reflected component. The solar radiation incident to an exposed horizontal surface was measured directly at each end of the canal. During times when the entire water surface was exposed to the sun, the percentage of the incident solar radiation to be reflected was determined by use of the expression:

$$R=1.18\ S_a^{-0.77} \tag{8}$$

in which R=reflectivity and S_a=sun altitude in degrees (Anderson, 1954). Equation 8 was developed for clear sky conditions, but it is used here under all weather conditions. Cloud cover, which was fairly rare, appears to have a fairly small effect on the reflectivity for sun altitudes above 30°. For low sun altitudes, the water surface was shaded by high banks on either side of the canal. Shading was accounted for by increasing the reflectivity.

For the purposes of determining the shading due to the banks, the canal was assumed to flow directly south (fig. 1) and the top of the bank was assumed to be 16.38 m from the centerline of the channel. The average bank height was found to be 8.11 m, measured relative to the invert of the canal. For each time step, the location of the sun (azimuth and elevation) was determined. Knowing the sun's azimuth, an altitude for complete shading of the water surface and for complete exposure were determined. If the water

surface was completely shaded, the value of reflectivity was assumed to be 0.9. In other words it was assumed that the diffuse component of solar radiation (about 10 percent) would be available even in the shade. If the water surface was completely exposed, equation 8 was used to determine the reflectivity. The reflectivity was assumed to vary directly with the sun's altitude ranging from a value of 0.9 for complete shading to the value given by equation 8 for complete exposure.

The amount of incoming atmospheric radiation was measured directly. Unfortunately, this measurement proved to be very difficult, and reliable values are not available for all the 141 days. In some cases, the incoming atmospheric radiation was estimated by use of a method proposed by Koberg (1964). Three percent of the incoming atmospheric radiation was assumed to be reflected (Anderson, 1954).

The longwave radiation emitted by the water surface was computed using the Stefan-Boltzman law for blackbody radiation.

$$H_b=\epsilon\sigma(T+273.16)^4 \tag{9}$$

in which ϵ=emissivity for water (0.97); σ=Stefan-Boltzman constant for black-body radiation; and 273.16 converts to the kelvins when the water temperature, T, is given in degrees Celsius.

The energy added by rainfall, which was a very rare occurrence, was determined by

$$H_R=c\rho i(T_w-T_b) \tag{10}$$

in which i=rainfall rate; T_w=wet-bulb air temperature; and T_b is an arbitrary reference temperature which is taken to be zero.

The other terms in equation 7 are related to the rate of evaporation, E. The thermal energy utilized by evaporation is expressed as

$$H_e=\rho L\psi(e_o-e_a) \tag{11}$$

in which L=latent heat of vaporization of water.

Heat exchange by conduction has received relatively little attention because its magnitude is usually small in comparison to the evaporation heat exchange. Assuming that eddy diffusivities of heat and mass are equal, which leads directly to the Bowen ratio concept, the conduction term can be expressed as

$$H_h=\gamma\rho L\psi)T-T_a) \tag{12}$$

in which γ=the psychrometric constant (0.0061 P_a); P_a=atmospheric pressure in kilopascals; and T_a=air temperature that should be measured at the same elevation as the vapor pressure.

The last term in equation 6 represents the thermal flux at the bed of the canal. In the past, attempts have been made to model the bed conduction term; the heat flux has been estimated to be the product of the thermal conductivity and the temperature gradient within the bed. Measurements of bed temperatures are difficult to take so are seldom available. In addition, bed conditions are seldom uniform. Even though the bed conduction term has been shown to be significant (Brown, 1969; Pluhowski, 1970) for shallow depths, it is usually ignored.

The concrete and earth under the San Diego Aqueduct were approximated as an infinitely thick conducting medium; the thermal properties of which were estimated. The thermal conductivity of flowing water is much greater, because of turbulence, than that of the concrete and soil; so the surface temperature of the bed can be assumed to equal water temperature.

Mathematical expressions for the temperature distribution and heat fluxes within a semi-infinite medium which result from an arbitrary temporal variation in surface temperature are relatively simple (Carlslaw and Jaeger, 1959, p. 64). Unfortunately, these expressions converge slowly and their use in a numerical model would be expensive. On the other hand, if the bed were considered to be a slab, insulated on the bottom and of an arbitrary thickness, Z, the equations are still fairly simple but converge much faster. If the temporal variations in surface temperature are cyclical, the heat fluxes determined by the semi-infinite and finite thickness slab equations become indistinguishable as the slab thickness increases. In fact, assuming a diurnal water temperature swing of 5°C and thermal properties for concrete, the surface heat fluxes for a slab only 25 cm thick are within 7 percent of the values for a semi-infinite medium.

The heat exchange between the water and the bed was, therefore, estimated by considering the bed to be a homogenous slab, insulated on the lower face and with a top-surface temperature equal to that of the overlying water. The heat flux into or out of the bed was then determined as a function of the past history of the water temperature. Only the thermal diffusivity and heat-storage capacity of the bed needed to be assumed. A slab thickness of 25 cm was assumed; this thickness is believed to be sufficiently thick to give the desired accuracy.

The temperature distribution within a slab, initially at constant temperature, for which the surface is subjected to a unit increase in temperature at time

zero is given by (Carslaw and Jaeger, 1959, p. 102)

$$\Delta T_B = 1 - \frac{4}{\pi} \sum_{n=0}^{\infty} \frac{(-1)^n}{2n+1} \exp\left[-k(2n+1)^2\pi^2 t/4Z^2\right] \cos\left[(2n+1)\,\pi y/2Z\right] \quad (13)$$

in which ΔT_B = the temperature rise within the slab; k = the thermal diffusivity; Z = thickness of the bed slab; and y = the distance above the insulated bottom of the slab at which temperature (ΔT_B) is computed. The increase in the heat content of the slab can be evaluated at any time by multiplying equation 13 by the heat-storage capacity, then integrating over the total thickness

$$H(t) = C_v Z \left(1 - \frac{8}{\pi^2} \sum_{n=0}^{\infty} \frac{(-1)^n}{(2n+1)^2} \exp\left[-k(2n+1)^2\pi^2 t/4Z^2\right] \sin\left[(2n+1)\,\pi/2\right]\right) \quad (14)$$

in which $H(t)$ = the increase in heat content of the slab between time 0 and t resulting from the unit increase in surface temperature at time zero; and C_v the heat-storage capacity of the slab which is the product of the density and specific heat. Of course this heat must have been provided from the overlying water.

Equation 6 is solved by use of a finite-difference approximation that advance in time by discrete steps of duration at DT. The heat flux from the slab to the water $\Delta H(i)$ during any time interval iDT to $(i+1)DT$ which results from a unit increase in water temperature at time zero, can be computed as

$$\Delta H(i) = H(iDT) - H\ [(i+1)\ DT]. \quad (15)$$

The $\Delta H(i)$'s describe the time variation of the response of the system to a unit change in water temperature.

Water temperature fluctuations can be approximated by a series of step changes, and the heat flux is linear with respect to temperature; so the superposition principle is used to determine the heat flux from the bed to the water for any temperature history by use of the equation

$$H_p(iDT) = \sum_{k=s}^{i} \Delta T(kDT)\ \ \Delta H(i-k) \quad (16)$$

in which $H_p(iDT)$ is the heat flux to the water from the bed during the time iDT to $(i+1)DT$; $\Delta T(kDT)$ is the change in water temperature which occurred at kDT ($k \leq i$); ΔH is given by equation 15; and the water temperature is assumed to have been constant for times before $t = (i-72)DT$. Equation 16 is solved for each cross section and each time step in a temperature model. The water temperature was assumed to have been constant before the model started ($\Delta T = 0$ for $k < 0$), and the bed conduction term was limited to a 24-hour memory ($s = i - 72$, since DT = 20 minutes).

Thermal diffusivity and heat-storage capacity of the bed material are the only additional parameters which are needed to include the bed conduction term in a thermal model. Heat-storage capacities are relatively easy to estimate. A thermal diffusivity of 0.01 cm²/s was found to work best for the concrete-lined canal.

No water was added to the canal, and the diversions had no effect on the temperature of the water remaining in the canal except insofar as they affected the depth and velocity. The effect of the diversions are accounted for in the flow model, and no special precautions were needed in the temperature model.

The flow and temperature models were coupled in that the output of the flow model was used as input to the temperature model. Hydraulic data at times midway between the time steps of the temperature model were obtained by straight-line interpolation between the values generated by the flow model.

The dispersion coefficient in equation 6 represents the combined results of several physical processes (Jobson and Yotsukura, 1973), and the estimation of its value is difficult. Fortunately, the predicted temperatures are not very sensitive to the assumed value of the dispersion coefficient. Figure 2 is presented to illustrate this insensitivity. The temperature measured at the downstream end of the San Diego Aqueduct on August 18, 1973, is shown in the figure, as well as the predicted temperatures obtained by solving equation 6 with two different values of the dispersion coefficient, D_x. One value of D_x was assumed to be equal to 7,500 $R_h U_*$, where U_* is the shear velocity and the other assumed $D_x = 250\ R_h U_*$. Changing the dispersion coefficient by a factor of 30 changed the predicted temperature at any time by less than 0.08 Celsius degree. The vertical scale, in figure 2, has been expanded during part of the day to illustrate that the value of 7500 $R_h U_*$ appears to overly smear small temperature variations. The large dispersion coefficient was observed in the Missouri River by Yotsukura, Fischer, and Sayre (1970), and the small value represents the approximate mean of all the measured values summarized by Fischer (1973). A value of $D_x/R_h U_* = 250$ is used throughout this report and the value of R_h was evaluated for the section near the center of the canal reach.

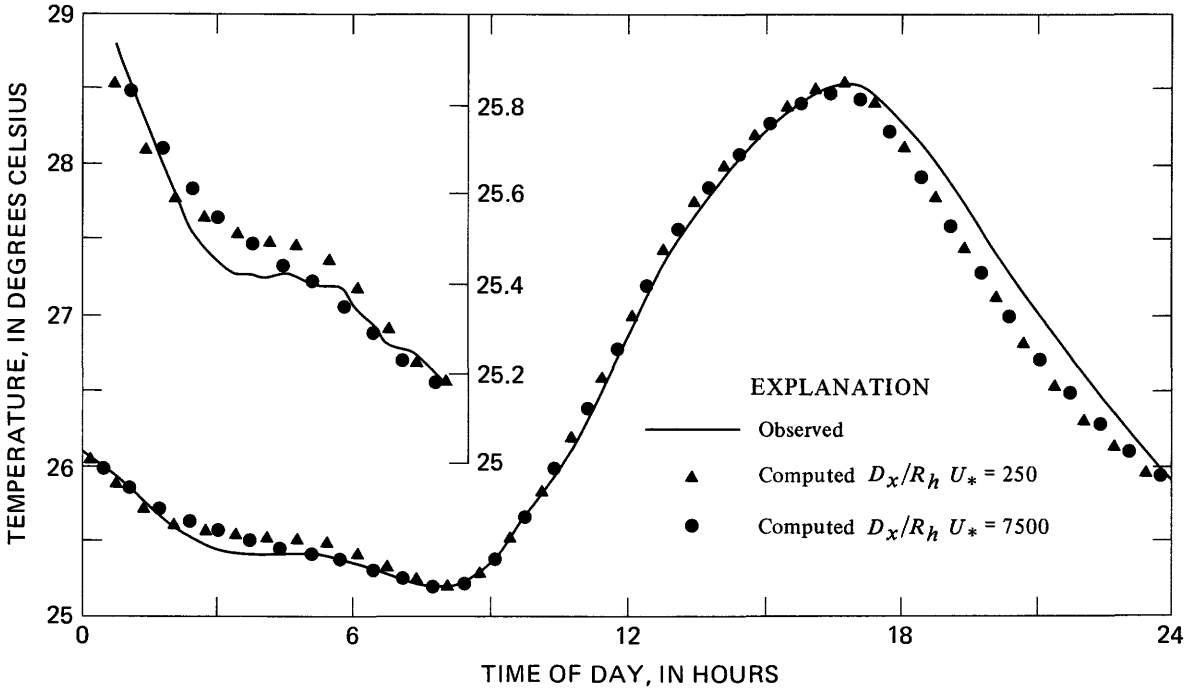

FIGURE 2.—The effect of the dispersion coefficient on the computed temperatures in the San Diego Aqueduct on August 18, 1973, in comparison with measured temperatures.

THE LAGRANGIAN MODEL

Equation 6 is an Eulerian equation, meaning that it is a description of the variation of temperature with respect to a fixed coordinate system. Another description, the Lagrangian, considers the variation of the temperature of a given parcel of fluid or fluid lump, as the parcel moves through the system. In the Lagrangian framework, one conceptually follows an individual fluid parcel while keeping track of the factors which tend to change its temperature. Applying the thermal continuity equation to a unit mass of fluid, the Lagrangian equivalent of equation 6 is

$$\frac{dT}{dt} = D_x \frac{\partial^2 T}{\partial x^2} + \frac{H_T W}{Ac\rho} + \frac{H_p}{R_h c\rho} \qquad (17)$$

Integrating both sides of equation 17 over the travel-time, one obtains

$$T_o - T_i = \int_o^\tau \left(D_x \frac{\partial^2 T}{\partial x^2} + \frac{H_T W}{Ac\rho} + \frac{H_p}{R_h c\rho} \right) dt \qquad (18)$$

in which T_o = final temperature of the water parcel as it passes the downstream end of the channel reach; T_i = initial temperature of the water parcel as it enters at the upstream end of the reach; and τ = travel-time required for the parcel to be convected through the system. Expanding the right-hand side of equation 18 yields

$$T_o - T_i = \int_o^\tau D_x \frac{\partial^2 T}{\partial x^2}\, dt + \int_o^\tau (H_N - H_b + H_R) \frac{W}{Ac\rho}\, dt + \int_o^\tau \frac{H_p}{R_h c\rho}\, dt - \int_o^\tau \psi \{L(e_o - e_a) + \gamma L(T - T_a)\} \frac{W}{Ac}\, dt. \qquad (19)$$

Equation 19 is extremely useful to a modeler because it allows the contribution of each exchange process to be isolated and evaluated. For example, integrating the first term in the second integral would determine the net temperature rise of a parcel due to absorbed atmospheric and solar radiation. Comparison of this value to the total temperature change $(T_o - T_i)$ then is a measure of the sensitivity of the predicted temperatures to errors in measurements of solar or atmospheric radiation.

One of the main purposes of this report is to determine the coefficients in the wind function which are applicable to the San Diego Aqueduct. Equation 19 provides a powerful tool for investigating the wind function. To make use of this tool we must assume that the wind function, ψ, applicable to a particular water parcel, is constant. Solving for the wind function by factoring it out of the integral gives

$$\psi = \frac{T_i - T_o + \int_o^\tau \left\{D_x \frac{\partial^2 T}{\partial x^2} + (H_N - H_b + H_R) \frac{W}{Ac\rho}\right\} dt + \int_o^\tau \frac{Hp}{R_h c\rho}\, dt}{\int_o^\tau \left\{L(e_o - e_a) + \gamma L(T - T_a)\right\} \frac{W}{Ac}\, dt} \quad (20)$$

The wind function in equation 20 is computed as a residual in that it is the average value which must be used during the traveltime, τ, to force the energy budget of the Lagrangian parcel to balance. Any measurement error or any physical process which is not correctly modeled will manifest itself as an error, or scatter, in the value of the wind function computed by use of equation 20. Nevertheless, if measurements are carefully made on a well-selected site, the results can be consistent and useful.

Before equation 20 can be solved, the variation of water temperature with time and distance must be known or assumed. The resulting wind function value, however, is not very sensitive to this water temperature distribution. Equation 6 was used, before the application of equation 20, to estimate the internal water temperature distribution. In the solution to equation 6, the wind function was assumed to be related to the windspeed as shown in equation 2. The final result was obtained by use of an iterative process in which (a) the coefficients in equation 2 were assumed; (b) equation 6 was solved for the 28-day calibration period; (c) equation 20 was solved for the wind function at 1,890 equally spaced times during the calibration period; (d) the wind function values were plotted against the windspeeds representative of the time of passage of the water parcel and new estimates of the coefficients in equation 2 obtained; and (e) if the new estimates were significantly different from the previous estimates, the process was repeated. Equations 6 and 20 were solved using numerical techniques and the process converged very rapidly. Each term in equation 20 was calculated separately so that the relative contribution of each physical process to the total temperature changes of any particular fluid parcel could be determined.

DATA AND MODEL CALIBRATION

DATA AVAILABLE

Meterologic data including incoming solar radiation, incoming atmospheric radiation, windspeed, wind direction, air temperature, and wet-bulb air temperature, were continuously recorded at each end of the canal for a 1-year period beginning July 25, 1973. In addition, the water temperature at each end, the depth at five locations, and the flow rate were continuously monitored.

The water temperature and all meteorologic data, except rainfall which was a rare occurrence, were recorded every 10 minutes in digital form on magnetic tape. The five stages were recorded continuously on analog charts. The charts were digitized to give hourly stages. During times of steady flow, the discharges were furnished by the Metropolitan Water District from current-meter measurements and (or) gate ratings. After February 28, 1974, a continuous analog record of discharge was available from a sonic flow meter. Before February 29, 1974, unsteady flow rates were computed from Manning's equation using the farthest upstream stage measurement. The roughness coefficient applicable in the Manning equation was determined during the periods of steady flow.

For further information concerning the site layout or the data collection effort, the reader is referred to Jobson and Sturrock (1976).

Because of equipment malfunctions and times when there was no flow in the canal, the data for all 365 days of the study were not complete. A total of 141 days were judged to have sufficient data to calibrate or verify the thermal model. These 141 days existed in eight groups of continuous data. The length and dates for each group are shown in table 2. The smallest group contained 4 consecutive days and the largest group 45 days. To be considered acceptable for analysis, certain criterion had to be met. These were:

1. The water temperature must be available at both ends of the canal.
2. Flow data must be reasonably complete.
3. All meterologic parameters, except atmospheric radiation, must be available at either the Cottonwood (upstream) or the Skinner (downstream) station.

Even during the 141 days, many time periods of short duration existed for which the data were not complete. For example, there were frequent gaps in the wet-bulb temperature record because the wick of the wet-bulb probe dried out for short periods of time. Because the model requires a complete data set for operation, the observed data were copied on a temporary data file and all missing or questionable data were filled in or replaced before the model was run. If a parameter was missing for only an hour or so, the missing values were interpolated. If a longer period of record was missing, the missing values were assumed to be equal to the values observed at the other station.

TABLE 2.—*Summary of modeled data for the San Diego Aqueduct*

[RMS = root mean square]

Group of data	Beginning		Ending		Length of record in hours	Error in computed temperature (°C)		Mean daily flow rate, in cubic meter per second	
	Date	Hour	Date	Hour		Mean	RMS	Mean	Standard deviation
1	07-25-73	1440	08-21-73	0400	638	+0.01	0.14	13.03	0.41
2	11-28-73	1720	12-12-73	1440	334	− .08	.23	6.65	1.58
3	12-19-73	1000	12-24-73	1140	122	− .16	.22	11.10	.69
4	03-07-74	2220	03-10-74	1200	62	+ .01	.12	23.58	.56
5	03-13-74	920	03-21-74	2400	207	− .04	.14	19.36	5.30
6	04-18-74	1020	05-01-74	1240	314	− .07	.22	13.95	1.07
7	05-08-74	1520	06-22-74	1420	1079	− .16	.26	15.98	1.35
8	07-05-74	1040	07-23-74	1420	436	− .13	.23	20.34	.20

Vapor pressures and wet-bulb temperatures were handled with special care. Vapor pressures were computed from the observed wet- and dry-bulb temperatures at both stations before any missing records were filled. Then the vapor pressure was treated as if it were a measured parameter so that in no case was the vapor pressure computed from wet- and dry-bulb temperatures obtained at different locations.

It was observed that the diurnal range in atmospheric radiation differed depending upon the sensor type (Eppley or Gier-Dunkle)[1] used in its detection. Although daily mean values appeared consistent, the observed diurnal variation appeared to be too large for both sensor types (Jobson and Sturrock, 1976). It was assumed, therefore, that the incoming atmospheric radiation did not vary during a day, and the daily average value was used. During the calibration period July 25, 1973, to August 21, 1973, the atmospheric radiation was observed at both ends of the canal by use of Eppley pyrgeometers. Between November 28, 1973, and March 10, 1974, only the Eppley pyrgeometer at Skinner was used. After March 13, 1974, the incoming atmospheric radiation component was estimated by use of the procedure outlined by Koberg (1964).

MODEL CALIBRATION

No flow model calibration, as such, was involved in this study. As stated previously, the flow was unsteady for only 5 of the 141 days, and the stage was continuously monitored at five points along the canal length. The mean and standard deviation between the daily average flow rates for each data group is shown in table 2. Knowing the flow rate into the canal, as well as the canal depth as a function of time and distance (from eq. 3), the discharge at any point and time was uniquely determined from continuity considerations (eq. 5). In order to illustrate the response of the system to a typical transient, the observed stages as well as the discharge values at the inlet and outlet are shown in figure 3 for transients which occurred on December 10–11, 1973. The Cottonwood, Simpson, Newport, South End, and Skinner gages are 0.3, 9.1, 13.5, 25.0, and 26.0 km downstream of the canal entrance respectively. The Cottonwood discharge is computed from the observed stage at Cottonwood, and the Skinner discharge is determined from equation 5.

Before October 1, 1973, the roughness of the canal was observed to be constant with a value of 0.0175 but after October 1, the observed roughness appeared somewhat erratic (Jobson and Sturrock, 1976, p. 69). The results of the thermal model obtained for the second period, November 28 to December 12, 1973, seemed to be more consistent when the roughness was assumed to be 0.0175 than when it was assumed to be 0.0151 as published by Jobson and Sturrock (1976). Therefore, the results for this period were obtained by assuming the Manning's roughness coefficient to be 0.0175.

The modeled and observed temperatures on the 5 days when unsteady flow occurred were critically reviewed, but no systematic error that appeared to be related to inadequate flow model results could be detected. A sensitivity analysis, conducted in some preliminary runs during the calibration period, indicated that neither the RMS (root-mean-square) error in predicted temperatures nor the derived coefficients in the wind function were extremely sensitive to discharge errors. A one percent increase in computed discharge increased the intercept coefficient, α, in equation 2 by about 4 percent and decreased the mass-transfer coefficient, N, by about 4 percent.

It was also determined by a sensitivity analysis of data input for the calibration period that the intercept was not very sensitive to errors in the measured solar radiation or the assumed thermal diffusivity of the bed, but that it was fairly sensitive to errors in the observed atmospheric radiation. A one percent increase

[1]The use of brand names in this report is for identification purposes only and does not imply endorsement by the U.S. Geological Survey.

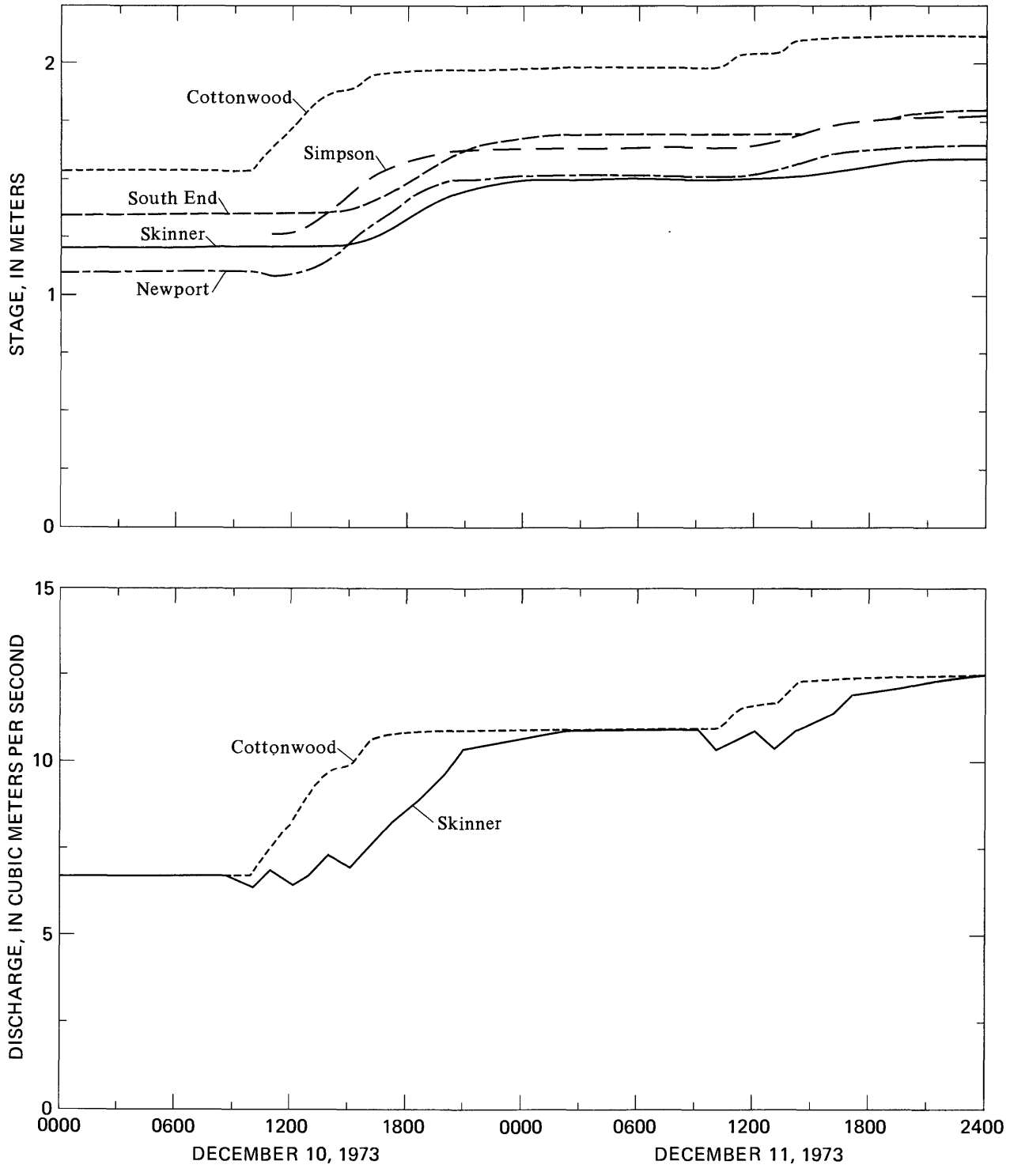

FIGURE 3.—Variation of stage and discharge for the flow transients on December 10 and 11, 1973.

in the values of solar radiation, atmospheric radiation, and thermal diffusivity changed the intercept by +0.4, +3, and 0.1 percent, respectively. The fitted mass-transfer coefficient, on the other hand, was somewhat sensitive to errors in solar radiation but not to errors in atmospheric radiation or bed diffusivity. One percent increases in solar radiation, atmospheric radiation, and thermal diffusivity changed the mass-transfer coefficient by +2, +0.6, and −0.02 percent, respectively.

In summary, the computed coefficients in the wind function were sensitive to certain measured parame-

ters such as flow rate and radiation, but measurement errors were not unreasonably amplified.

The RMS error in computed temperatures was not very sensitive to assumed value of thermal diffusivity of the bed as long as it was within the range of 0.008 cm^2/s to 0.015 cm^2/s. Outside this range, the RMS error increased rapidly. By comparison, the range of thermal diffusivities observed in concrete dams on the Tennessee River was from 0.0061 cm^2/s for Bull Run Dam to 0.0141 cm^2/s for Norris Dam (Troxell and others, 1956). If the assumed thermal diffusivity was outside the indicated range, the computed values of the wind function did not appear to be linearly related to windspeed. Figure 4 illustrates the effect of thermal diffusivity on the wind function values computed for July 30, 1973. With the diffusivity set equal to zero, the wind function values for the day define a loop rather than a straight line. Assuming diffusivities larger than 0.015 cm^2/s also created a loop, but the loop progressed counterclockwise with increasing time.

Equation 20 was solved for the wind function at 1,890 equally spaced times during the 28-day calibration period. The average windspeed, during the transit of each parcel, was also tabulated, and the wind function values were plotted as a function of windspeed. The results are shown in figures 5 through 11. Also shown in each illustration is a straight line of best fit for the day as well as the correlation coefficient.

A composite of all of the results shown in figures 5–11 is shown in figure 12 along with the equation

$$\psi = 3.02 + 1.13\ V \qquad (21)$$

in which the wind function is given in millimeters per day per kilopascal when the windspeed, V, is given in meters per second. Equation 21 was derived by use of a regression analysis on all 1,890 values of windspeed and wind function during the calibration period, and it was used in equation 6 for all days in the analysis procedure. Equation 21 is considered to be the principal result of this study.

An idea of the total variability of the wind function can be obtained from figure 12. As can be seen from

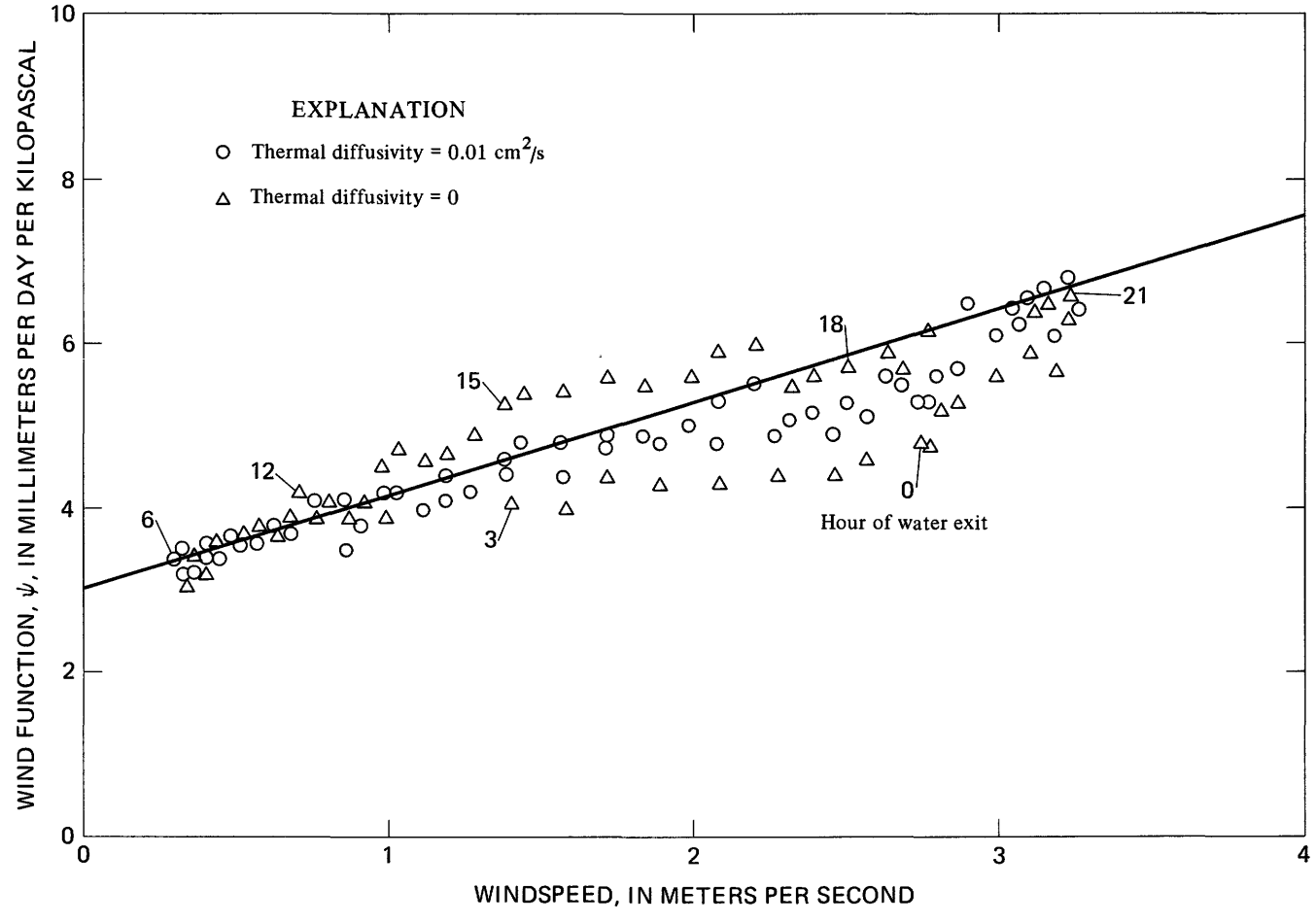

FIGURE 4.—Comparison of wind function values for July 30, 1973, as computed with and without heat transfer between the water and the bed.

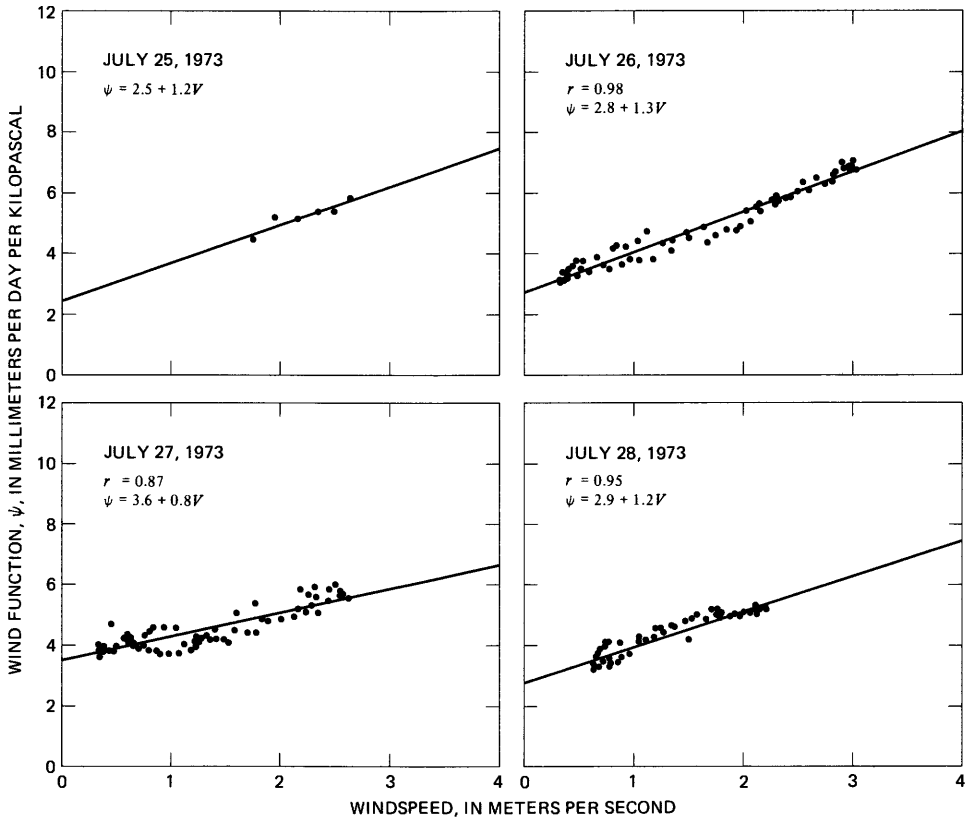

FIGURE 5.—Variation of the wind function, with windspeed for the San Diego Aqueduct during July 25 through 28, 1973.

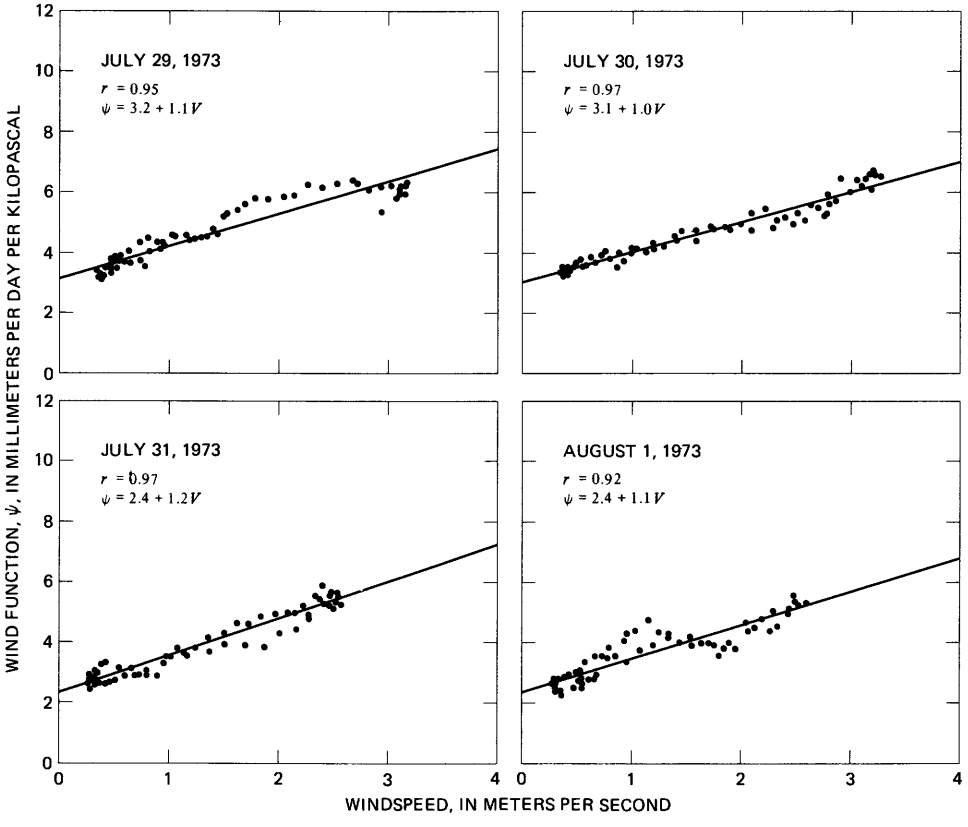

FIGURE 6.—Variation of the wind function, with windspeed for the San Diego Aqueduct during July 29 through August 1, 1973.

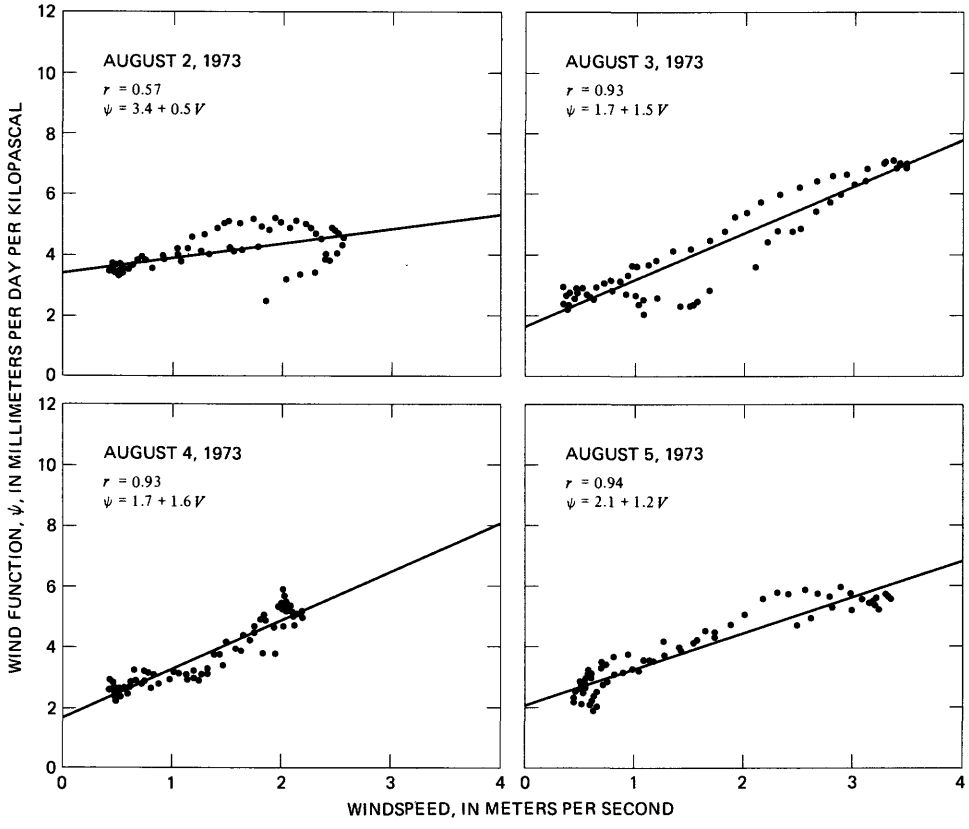

FIGURE 7.—Variation of the wind function, with windspeed for the San Diego Aqueduct during August 2 through August 5, 1973.

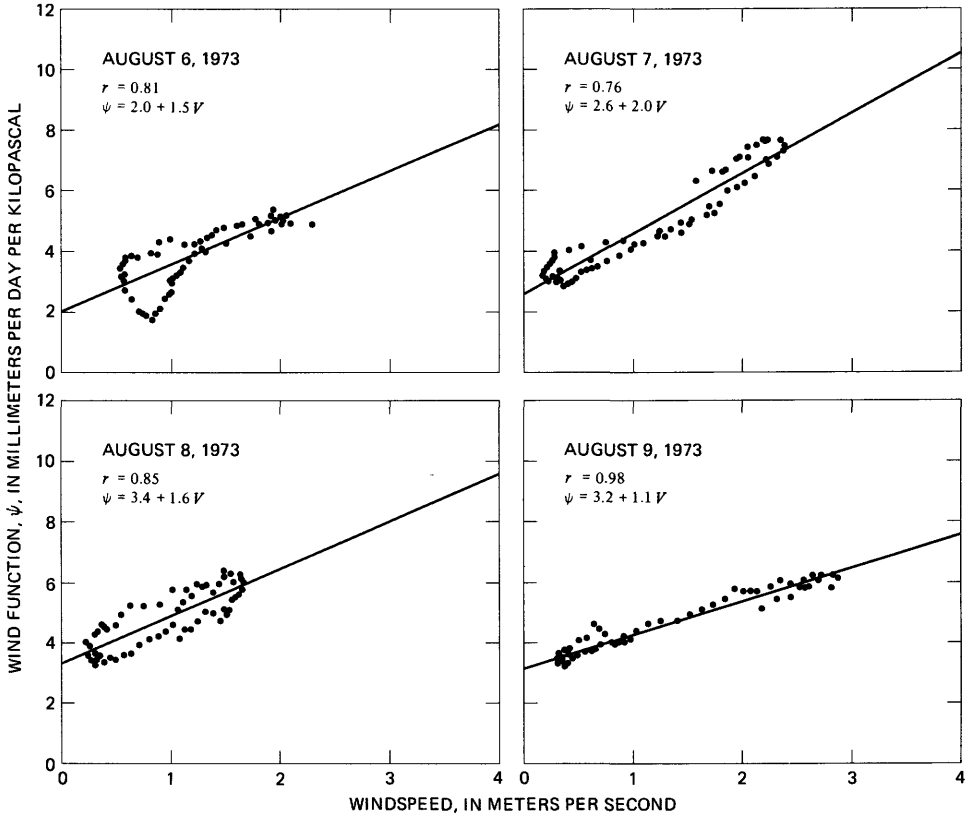

FIGURE 8.—Variation of the wind function, with windspeed for the San Diego Aqueduct during August 6 through August 9, 1973.

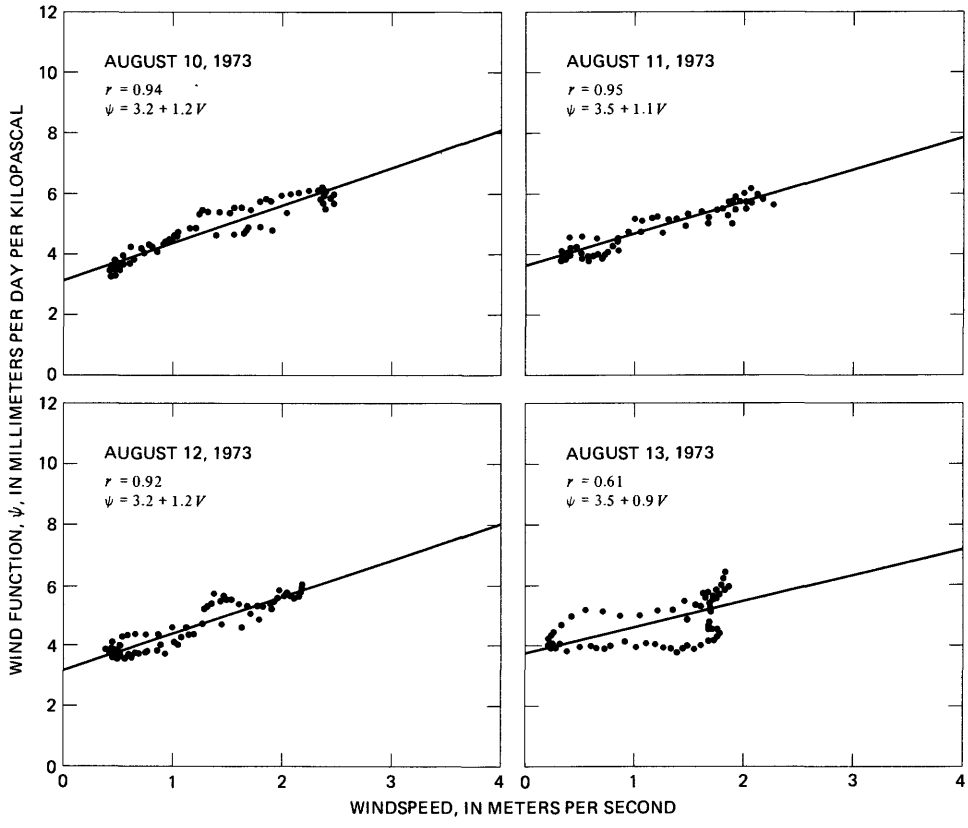

FIGURE 9.—Variation of the wind function, with windspeed for the San Diego Aqueduct during August 10 through August 13, 1973.

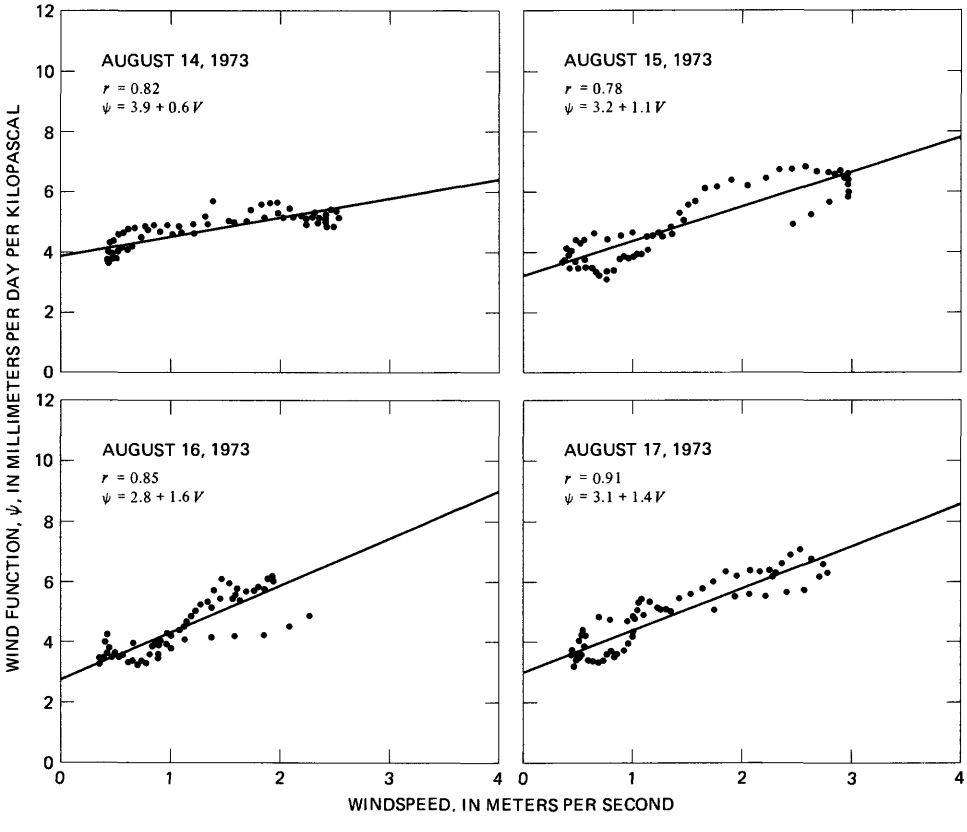

FIGURE 10.—Variation of the wind function, with windspeed for the San Diego Aqueduct during August 14 through August 17, 1973.

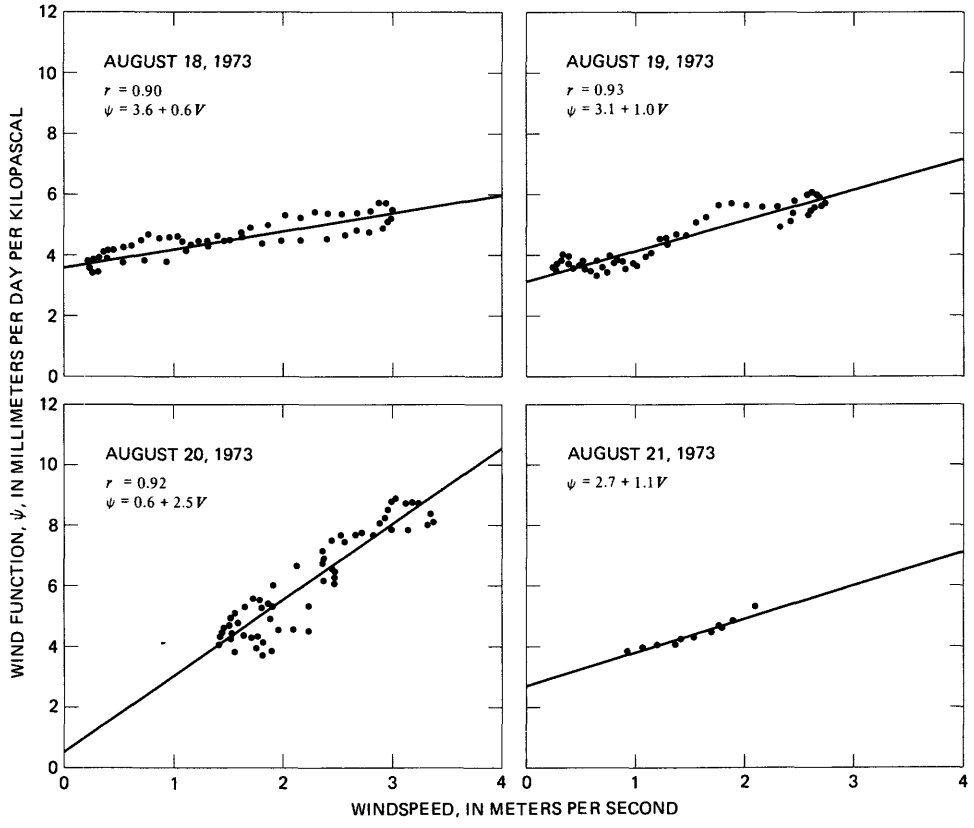

FIGURE 11.—Variation of the wind function, with windspeed for the San Diego Aqueduct during August 18 through August 21, 1973.

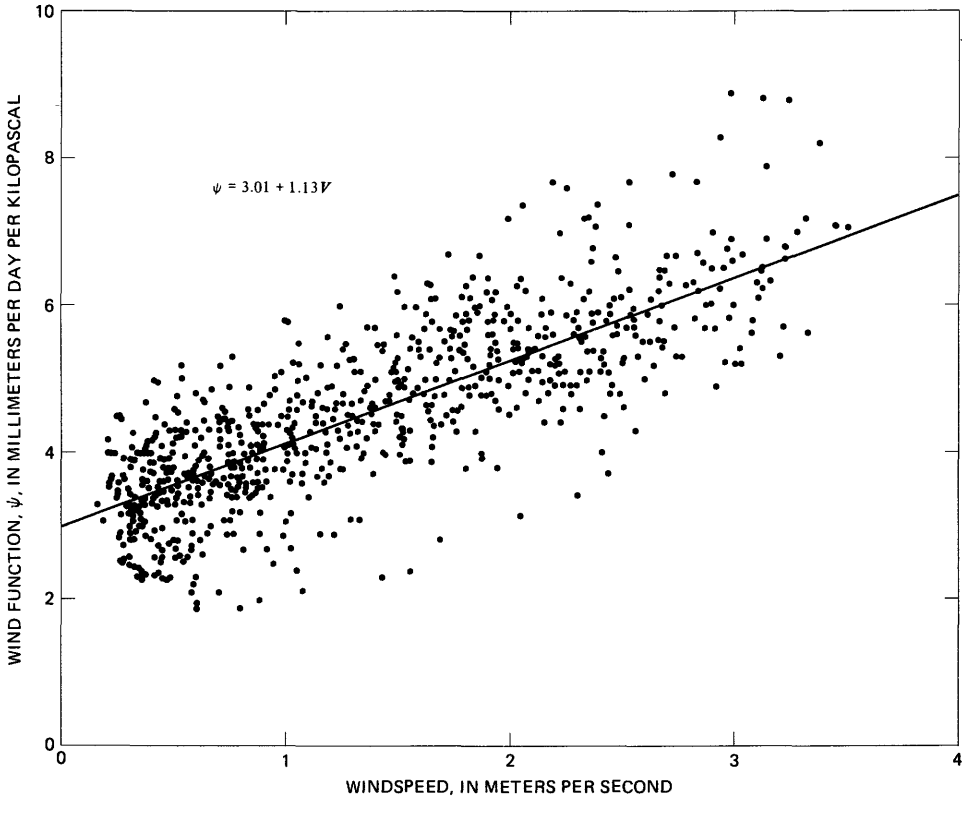

FIGURE 12.—Computed wind function values for the San Diego Aqueduct. Every other point plotted for the 28-day period starting July 25, 1973.

figures 5 through 11, the data for any particular day generally defines a reasonably straight line, but the mass-transfer coefficient and intercept varies from day to day. Ignoring the results for 2 of the 26 complete days, the intercept varies from 1.7 to 3.9 and the mass-transfer coefficient varies from 0.5 to 1.6. Nevertheless, equation 21 seems to be fairly well defined by the data and indeed it is entirely possible that the intercept and mass-transfer coefficient are somewhat dependent on wind direction or other meteorologic factors which vary from day to day.

With the wind function defined by equation 21, equation 6 was capable of predicting the downstream temperature during the 28-day calibration period with a RMS error of 0.14°C. A sample of the predicted and measured temperatures is shown in figure 13.

MODEL VERIFICATION AND DISCUSSION

The ability of equation 21 to accurately define evaporation from the San Diego Aqueduct was verified by solving equation 6, wherein the wind function is defined by equation 21, for the remaining 113 days of data. These days were scattered throughout the year and included days in the months of November, December, March, April, May, June, and July. Visual verification with typical results is illustrated in figures 14 through 20 which contain the observed and modeled temperatures during the first 4 full days of each of the seven groups of verification data. The mean and the RMS error in the predicted temperatures for each group are shown in table 2. The overall RMS error during the 113 days of verification is 0.23°C.

Errors tend to be smaller during the winter; this should be expected because of the smaller diurnal range. The observed temperatures during March 1974 (figs. 16 and 17) appear somewhat erratic possibly because of instrumentation errors. The temperature recorder at the lower end of the canal definitely malfunctioned soon after March 21, 1974. Overall, the

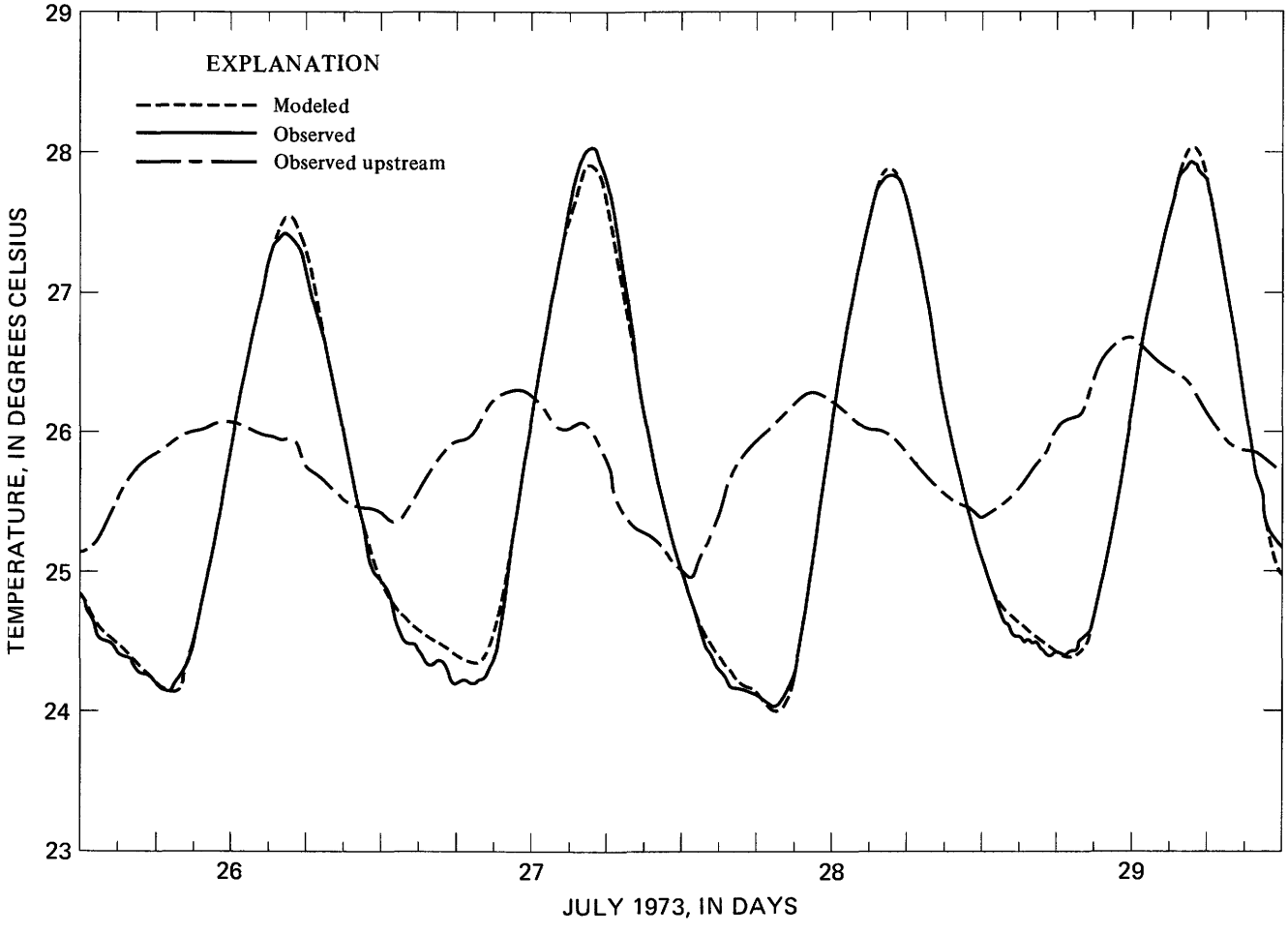

FIGURE 13.—Comparison of the modeled and observed temperatures at the downstream end of the San Diego Aqueduct during the first 4 days of the calibration period.

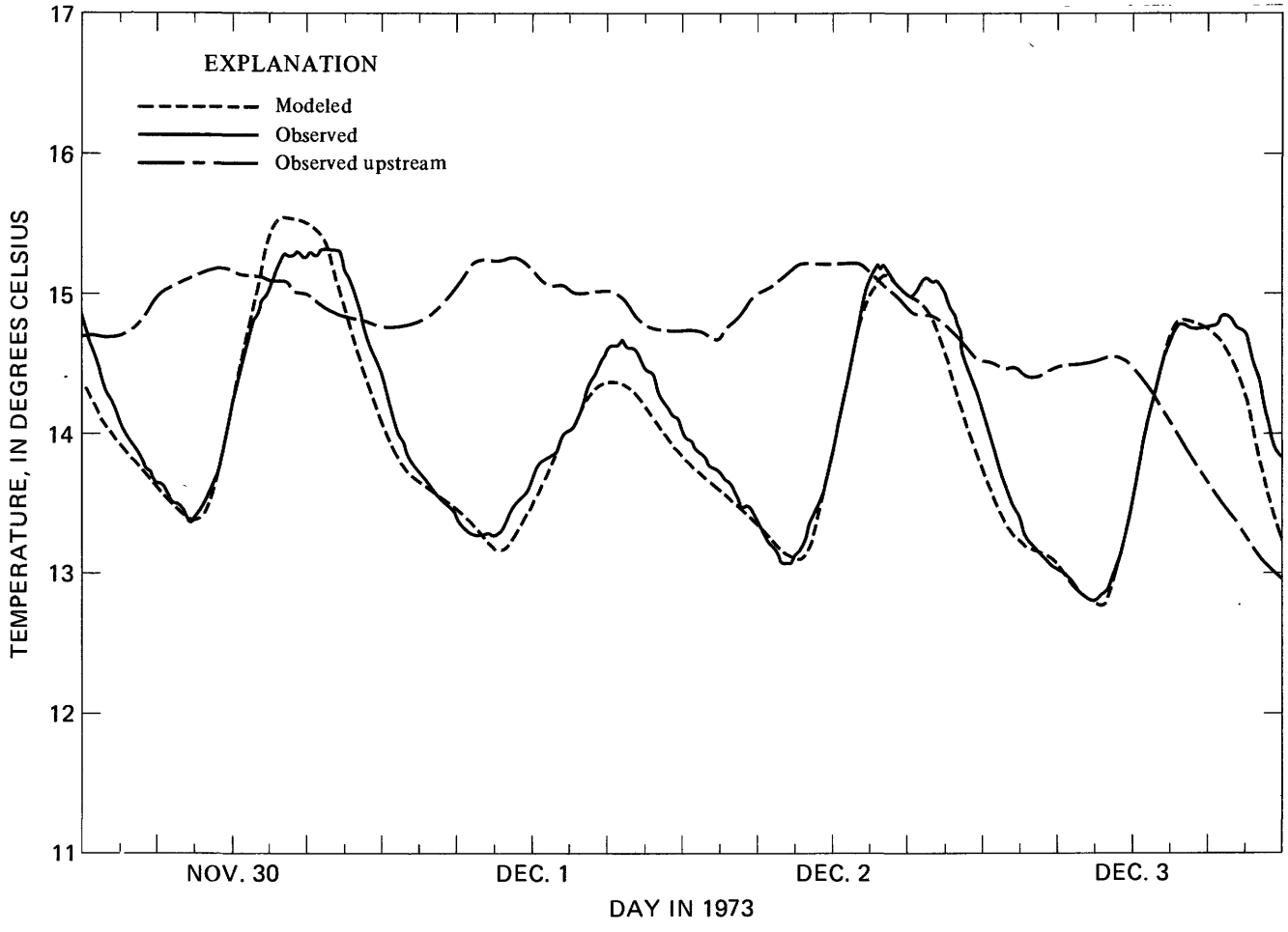

FIGURE 14.—Comparison of the modeled and observed temperatures at the downstream end of the San Diego Aqueduct during the first 4 days of the first verification.

results of the verification appear to be very good.

The results illustrated in figures 14–20 are believed to verify that equation 21 predicts representative evaporation rates during all seasons of the year. On the other hand, the results shown in figures 5 through 11 suggest that the wind function coefficients in equation 21 vary from day to day. In order to determine if these coefficients varied in any systematic manner throughout the year, equations 6 and 20 were solved simultaneously for the seven verification periods in the same manner as for the calibration period. Plots similar to those shown in figures 5–11 were inspected, and the daily values of the wind function coefficients were determined. Table 3 contains a tabulation of the results for all days in which the correlation coefficients for the linear regression exceeded 0.7. Fewer results are shown for the cooler months. During this time, evaporation became a small factor in the energy budget so that random errors in the other components were amplified. Although significant scatter in the daily mass transfer coefficients exist, no seasonal pattern is apparent. The intercept values, on the other hand, appear to increase between March and July. Since the intercept values are fairly sensitive to errors in the atmospheric radiation term and no actual measurements of this term was available after March 13, 1974, little emphasis is placed on the apparent trend.

Figures 13 through 20 demonstrate that equation 21 provides accurate predictions of water temperature when incorporated in a thermal model. But before the accuracy of equation 21 can truly be verified, it must be demonstrated that the accuracy of the predicted temperatures is reasonably sensitive to the evaporation rate. The diurnal variation in water temperature at the canal entrance is very small as can be seen in figures 13 through 20. The San Diego Aqueduct is fed by a pipeline which passes under the San Jacinto Mountains just upstream of the canal entrance. The ability of the model to start with a relatively constant inflow temperature and to accurately predict the diurnal swings at the downstream end implies that

TABLE 3.—*Daily values of the wind function coefficients for the San Diego Aqueduct*

Date	Intercept (α) [mm/d·kPa]	Mass transfer (N) [mm/d·kPa·m/s]	Correlation coefficient
07-26-73	2.80	1.30	0.98
07-27-73	3.60	.80	.87
07-28-73	2.90	1.20	.95
07-29-73	3.20	1.10	.95
07-30-73	3.10	1.00	.97
07-31-73	2.40	1.20	.97
08-01-73	2.40	1.10	.92
08-03-73	1.70	1.50	.93
08-04-73	1.70	1.60	.93
08-05-73	2.10	1.20	.94
08-06-73	2.00	1.50	.81
08-07-73	2.60	2.00	.76
08-08-73	3.40	1.60	.85
08-09-73	3.20	1.10	.98
08-10-73	3.20	1.20	.94
08-11-73	3.60	1.10	.95
08-12-73	3.20	1.20	.92
08-14-73	3.90	.60	.82
08-15-73	3.20	1.10	.78
08-16-73	2.80	1.60	.85
08-17-73	3.10	1.40	.91
08-18-73	3.60	.60	.90
08-19-73	3.10	1.00	.93
08-20-73	.60	2.50	.92
11-30-73	2.60	1.10	.72
12-11-73	2.50	1.80	.88
12-22-73	−.80	2.60	.84
03-18-74	−1.10	6.00	.88
03-20-74	−1.70	2.50	.74
03-21-74	−1.50	5.00	.81
04-19-74	−2.20	3.60	.80
04-20-74	1.10	2.50	.73
04-22-74	1.60	2.50	.86
04-23-74	1.40	1.70	.82
04-24-74	−2.00	3.00	.91
04-25-74	.80	1.60	.95
04-26-74	.50	2.00	.86
04-27-74	.30	2.40	.89
04-28-74	.80	2.10	.92
04-29-74	1.60	1.20	.72
05-10-74	−3.90	4.60	.92
05-11-74	−1.70	3.80	.95
05-12-74	.40	2.30	.84
05-13-74	−3.60	3.50	.91
05-16-74	−1.00	2.30	.92
05-17-74	−.70	2.40	.94
05-18-74	.60	1.70	.94

TABLE 3.—*Daily values of the wind function coefficients for the San Diego Aqueduct*—Continued

Date	Intercept (α) [mm/d·kPa]	Mass transfer (N) [mm/d·kPa·m/s]	Correlation coefficient
05-19-74	1.80	1.40	0.88
05-20-74	1.20	1.80	.90
05-21-74	1.40	1.50	.79
05-22-74	1.60	1.30	.83
05-23-74	1.90	1.00	.84
05-24-74	1.80	1.40	.71
05-26-74	2.60	3.60	.86
05-27-74	3.10	1.60	.97
05-28-74	1.20	1.60	.94
05-29-74	1.80	1.10	.92
05-31-74	.70	.90	.91
06-01-74	1.30	.90	.95
06-02-74	2.30	.60	.86
06-03-74	1.90	.90	.88
06-04-74	2.00	.80	.90
06-05-74	2.00	.80	.94
06-06-74	2.40	.80	.94
06-07-74	.10	1.00	.87
06-08-74	1.00	.90	.93
06-09-74	2.40	.40	.73
06-10-74	2.30	.60	.93
06-11-74	1.90	1.00	.88
06-12-74	1.50	1.30	.90
06-13-74	2.40	.90	.95
06-14-74	2.50	.60	.89
06-15-74	2.50	.40	.85
06-16-74	2.70	.80	.93
06-17-74	2.40	.70	.97
06-18-74	2.10	.80	.97
06-19-74	2.30	.80	.89
06-20-74	1.90	1.00	.94
06-21-74	2.30	.80	.97
07-06-74	2.80	.70	.97
07-07-74	2.00	.80	.97
07-08-74	1.50	1.20	.90
07-09-74	2.40	.80	.95
07-10-74	.80	1.50	.91
07-11-74	1.90	.90	.82
07-12-74	2.60	.50	.90
07-13-74	2.70	.60	.82
07-16-74	2.20	.80	.92
07-17-74	2.40	.50	.90
07-18-74	3.30	.60	.84
07-20-74	1.70	1.10	.89
07-21-74	1.90	.80	.94
07-22-74	1.70	2.00	.78

the surface exchange, including evaporation, is being accurately modeled.

The study site was selected such that it would be in a climate where a large part of the total surface exchange is due to evaporation. Equation 19 provided the means of evaluating the contribution of each process to the energy budget of an individual water parcel passing through the canal. In order to illustrate the relative contributions of each process, the mean and standard deviation of each major term in equation 19 are tabulated in table 4 for each group of data. It is seen that evaporation H_e, as well as the net radiation, $H_N - H_b$, are major components of the energy budget. Conduction to the air or the bed are small components. Comparing the RMS error in the predicted temperature (table 2) to the temperature change due to evaporation (table 4), it is seen, that except perhaps for a short period in March when there may have been instrument malfunction, the evaporation must have been modeled fairly well. It is concluded, therefore, that the evaporation from the San Diego Aqueduct is realistically represented by the wind function of equation 21.

In order to compare equation 21 with existing wind functions, a simple seventh-root velocity law was used to convert windspeeds for all equations to a common reference height of 4 m, which was the approximate height of the anemometers used in this study. No correction was made for the measurement height of the vapor pressure, and it was assumed that the effect of averaging data over periods of time of 1 day or less had no effect on the coefficients in the wind function.

TABLE 4.—*Summary of energy budget terms for individual water parcels passing through the San Diego Aqueduct*

Group	Beginning date	Mean and standard deviation of temperature increase, in degrees Celsius, to result from the indicated cause [Standard deviations in parentheses]					
		Observed temperature increase	Incoming radiation	Back radiation	Evaporation	Conduction to the air	Conduction to the bed
1	07–25–73	−0.21	2.78	−1.95	−1.00	0.0	0.00
		(0.86)	(1.00)	(0.05)	(0.35)	(0.16)	(0.09)
2	11–28–73	−0.54	3.12	−2.80	−0.71	−0.13	0.01
		(0.73)	(0.88)	(0.33)	(0.22)	(0.21)	(0.12)
3	12–19–73	−0.33	1.94	−1.82	−0.37	−0.08	0.01
		(0.55)	(0.56)	(0.02)	(0.15)	(0.11)	(0.06)
4	03–07–74	−0.22	1.20	−1.06	−0.25	−0.14	0.00
		(0.44)	(0.40)	(0.02)	(0.05)	(0.05)	(0.03)
5	03–13–74	+0.12	1.58	−1.31	−0.12	−0.02	0.00
		(0.62)	(0.69)	(0.29)	(0.25)	(0.19)	(0.05)
6	04–18–74	+0.01	2.53	−1.84	−0.58	−0.08	0.01
		(1.00)	(1.14)	(0.04)	(0.29)	(0.13)	(0.11)
7	05–08–74	−0.08	2.52	−1.82	−0.68	−0.08	0.01
		(0.98)	(1.11)	(0.22)	(0.31)	(0.13)	(0.09)
8	07–05–74	−0.06	2.27	−1.57	−0.72	0.0	0.00
		(0.86)	(1.04)	(0.03)	(0.35)	(0.13)	(0.08)

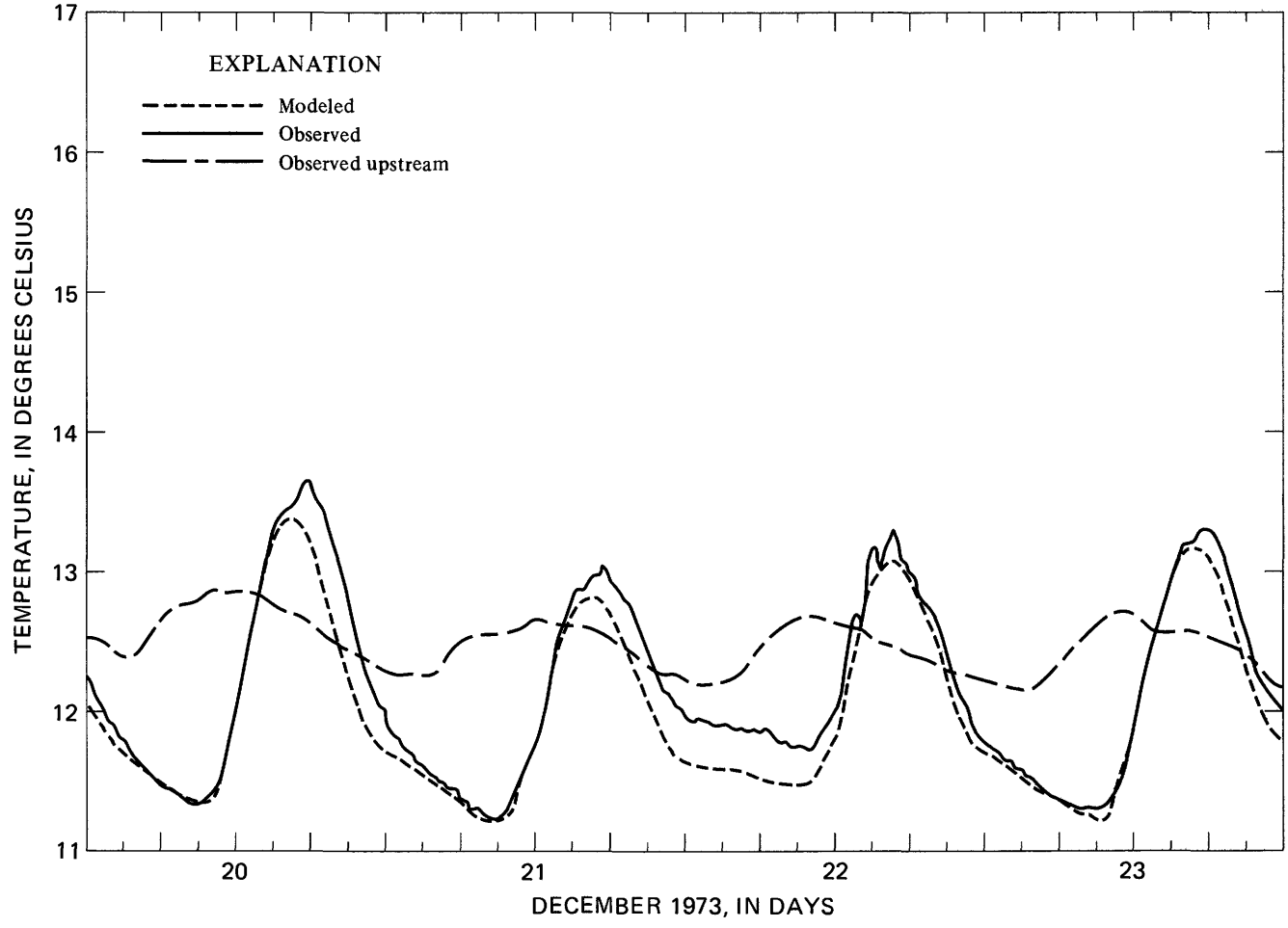

FIGURE 15.—Comparison of the modeled and observed temperatures at the downstream end of the San Diego Aqueduct during the first 4 days of the second verification.

Harbeck (1962) summarized evaporation studies made on reservoirs having little or no artificial heat inputs and having surface areas ranging from 4×10^3 to nearly $1.2\times10^8 m^2$. He proposed the relation

$$\psi = \frac{2.43}{A_r^{0.05}} V \quad (22)$$

in which A_r is surface area of the reservoir, in meters squared; and V is the windspeed at the center of the reservoir, in meters per second. The major difference between equation 21 and 22 is that Harbeck assumes no evaporation will occur unless a measurable windspeed exists. This is probably a reasonable assumption if the windspeed is measured near the center of a large lake, but it is probably unrealistic for computation of evaporation from streams. Near streams and rivers the rough terrain limits windspeeds to values less than the stall speeds of most anemometers during a fairly larger percentage of the time. In addition the flow velocity generates a relative motion between the water and air even at zero windspeeds. For a surface area of 150 m^2, (the average width of the canal was about 9 m) equations 21 and 22 intersect at a windspeed of about 4 m/s.

Above an artificially heated water surface, free convection may significantly increase the rate of evaporation. For artificially heated reservoirs, Ryan and Stolzenbach (1972) present the formula

$$\psi = 0.95(\Delta\theta)^{1/3} + 0.91V \quad (23)$$

in which $\Delta\theta$ is the difference between the virtual temperature of the air and the water surface. The virtual temperature is the temperature at which dry air would have the same density as the moist air mixture assuming constant pressure. They suggest that the value of $\Delta\theta$ should be taken as zero for water bodies with no thermal loading. The mass-transfer coefficients (slope) in equations 21 and 23 differ by 19 percent.

A commonly used formula was developed by Meyer in 1942 and published by Linsley, Kohler, and Paulhus (1958).

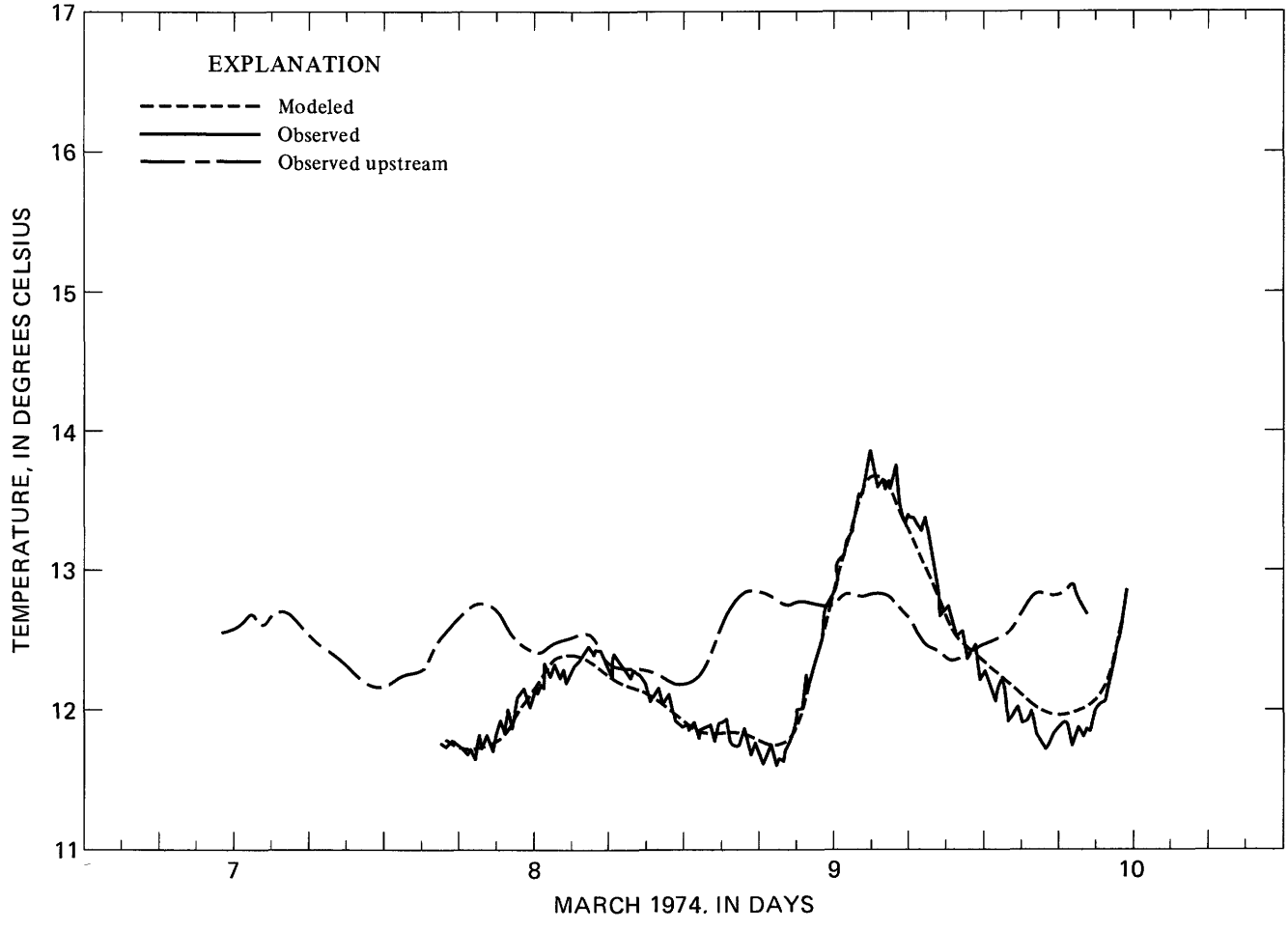

FIGURE 16.—Comparison of the modeled and observed temperatures at the downstream end of the San Diego Aqueduct during the third verification.

$$\psi = 2.7 + 0.66\ V. \qquad (24)$$

Although the mass-transfer coefficient is smaller, the intercept in formula 24 is only 11 percent less than that for equation 21.

The Tennessee Valley Authority (1972), as well as Ryan and Stolzenbach (1972), have given excellent summaries of many of the existing empirical wind function formulas. Equation 21 is, however, believed to be the only equation ever developed from the thermal balance of an open channel. In summary, the wind function for the San Diego Aqueduct (eq. 21) indicates a larger evaporation at low windspeeds than is indicated by most lake evaporation formulas, but the mass-transfer coefficient is within the range of values which have been reported. For the average windspeed at the San Diego Aqueduct, about 1.5 m/s, equation 21 indicates a slightly greater evaporation rate than would be indicated by most lake evaporation formulas.

In order to estimate the evaporative water loss from the San Diego Aqueduct, equations 1 and 21 were solved using daily averaged values of windspeeds, water temperature, and vapor pressure for each end of the canal (Jobson and Sturrock, 1976). The evaporative rate at each end of the canal was computed for each day, and the resulting monthly averaged evaporation rates were determined. The monthly average results are shown in figure 21 as well as in table 5. Because of missing data, mainly the vapor pressures of the air, a considerable amount of interpolation was required to estimate monthly evaporation rates. Using days when the daily average vapor pressure was available at both ends of the canal, a monthly value of the ratio of these vapor pressures was established. Missing vapor pressures were interpolated using these ratios as well as the monthly mean values and any other factors considered to be significant. Missing water temperatures were interpolated by paying special attention to the seasonal variation of the mean difference in the water temperatures at the ends of the canal. Very few windspeed data were missing.

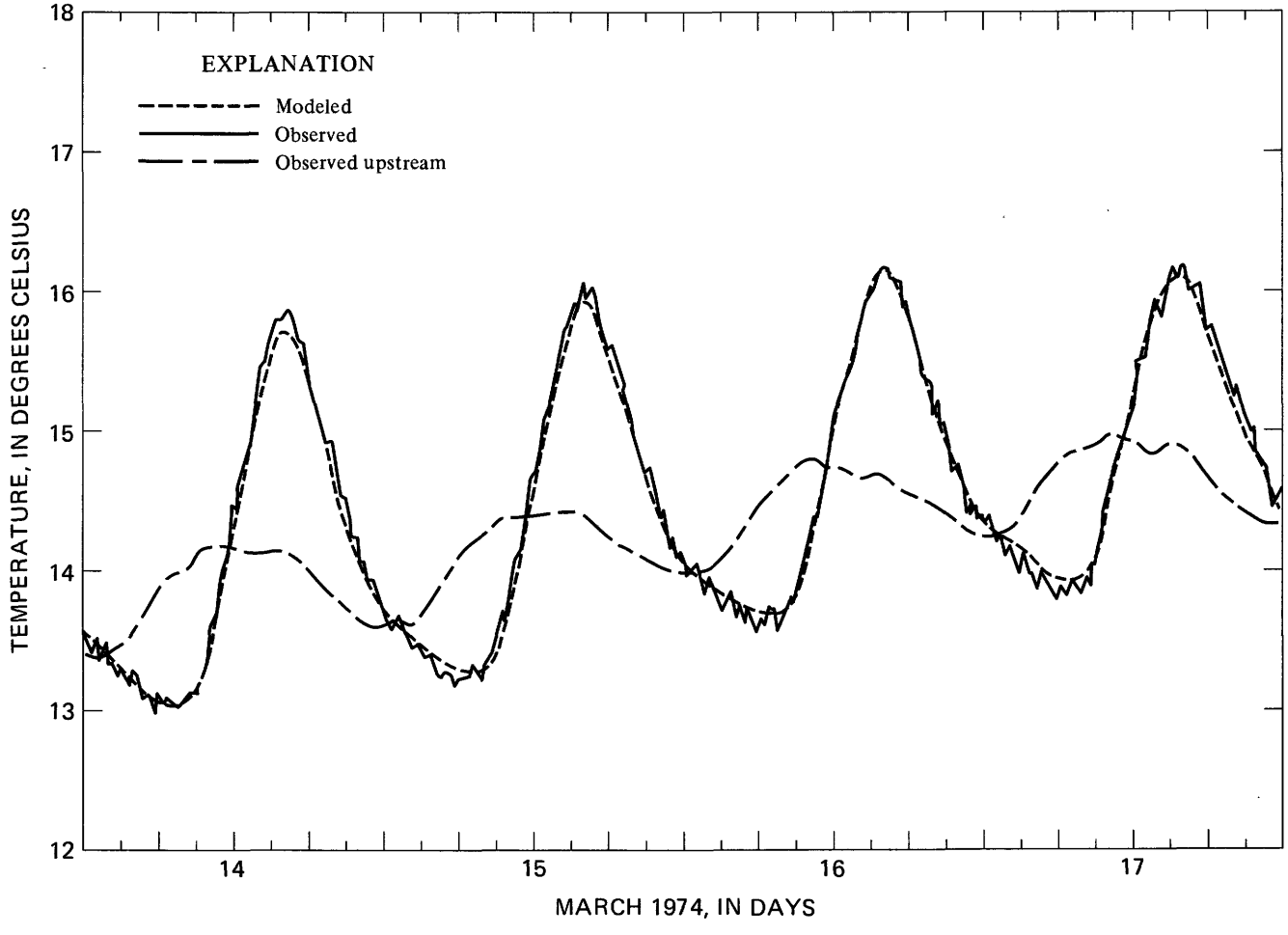

FIGURE 17.—Comparison of the modeled and observed temperatures at the downstream end of the San Diego Aqueduct during the first 4 days of the fourth verification.

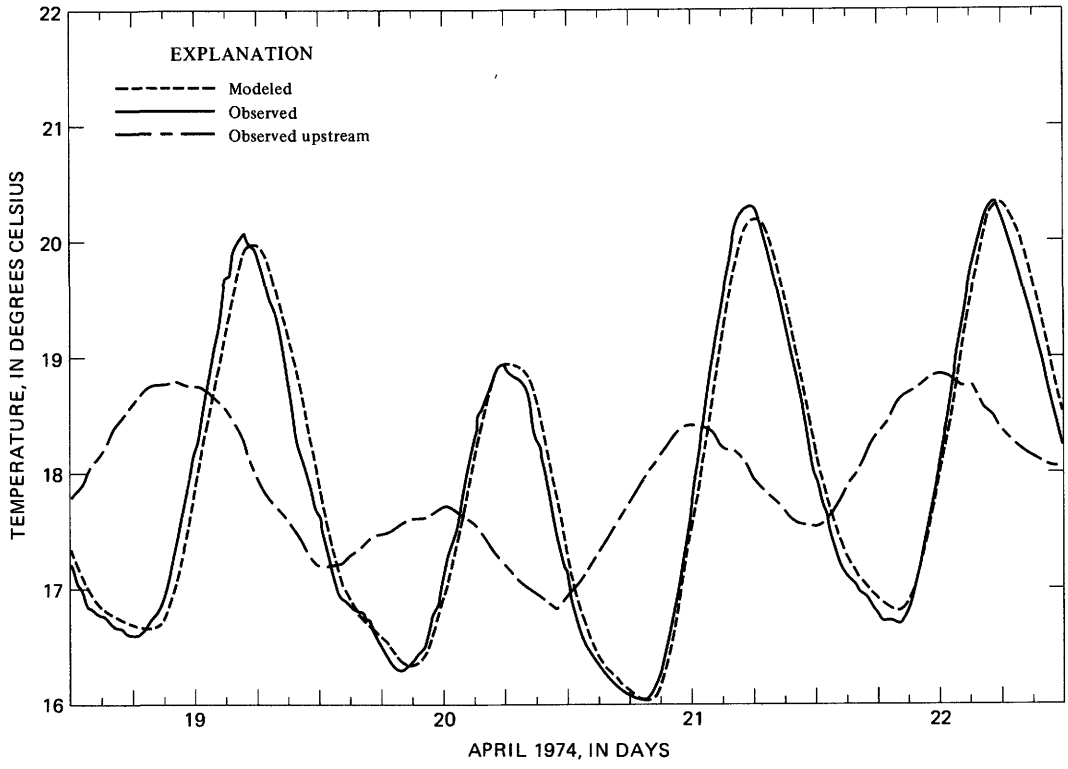

FIGURE 18.—Comparison of the modeled and observed temperatures at the downstream end of the San Diego Aqueduct during the first 4 days of the fifth verification.

The annual evaporation rate for the canal was estimated to be 2.08 m. This number is significantly larger than the estimated lake evaporation for the region of 1.32 m (Kohler and others, 1959) and slightly greater than the regional estimate for evaporation from a class A evaporation pan of 1.78 m. On the other hand, the average pan evaporation during the study, from class A evaporation pans maintained at each end of the canal by the Metropolitan Water District, is shown in table 5 along with the computed canal evaporation and a monthly pan coefficient. Assuming a pan evaporation of 8.3 mm/d during September, the annual pan loss was observed to be 2.29 m giving an annual observed pan coefficient of 0.91.

TABLE 5.—*Evaporation rates for the San Diego Aqueduct during the study period, July 25, 1973, to July 24, 1974*

Month	Evaporation rate in millimeters per day		Pan coefficient	Water loss by the Canal, in thousands of cubic meters
	Canal	Class A pan		
January	1.99	2.57	0.77	15.4
February	2.19	4.30	.51	4.3
March	2.47	3.45	.72	19.8
April	5.19	6.90	.75	43.7
May	6.62	6.97	.95	55.3
June	9.31	9.65	.96	78.2
July[1]	9.58	10.65	.90	81.6
August	7.96	9.80	.81	59.7
September	7.89	—	—	57.6
October	7.41	6.72	1.10	55.8
November	4.48	3.35	1.34	31.0
December	3.39	2.74	1.24	22.4
Total				524.8

NOTE:—1,000 m^3 = 0.811 acre feet.
[1]Represents composite of 1973 and 1974 data.

Comparing the computed canal evaporation with the observed pan evaporation values, one again reaches the conclusion that evaporation rate from the San Diego Aqueduct is a little greater than reservoir evaporation for the same area.

The evaporation rates estimated above were converted to water use by multiplying the average evaporation rate for each day by the effective surface area of the canal for that day. The surface area was computed from the mean daily stage values in conjunction with the shape of the canal and the data contained in table 1. The monthly water losses are also shown in table 5. The water loss for February is very low because the canal was empty during much of the month. Flow was continuous for all other months. The July value represents the loss during July 26–31, 1973, plus the loss during July 1–22, 1974, prorated to 31 days. Even during June, July, and August, the evaporative loss represents less than 0.2 percent of the total flow.

SUMMARY AND CONCLUSIONS

A one-dimensional temperature model has been developed by use of flow and meteorologic data collected

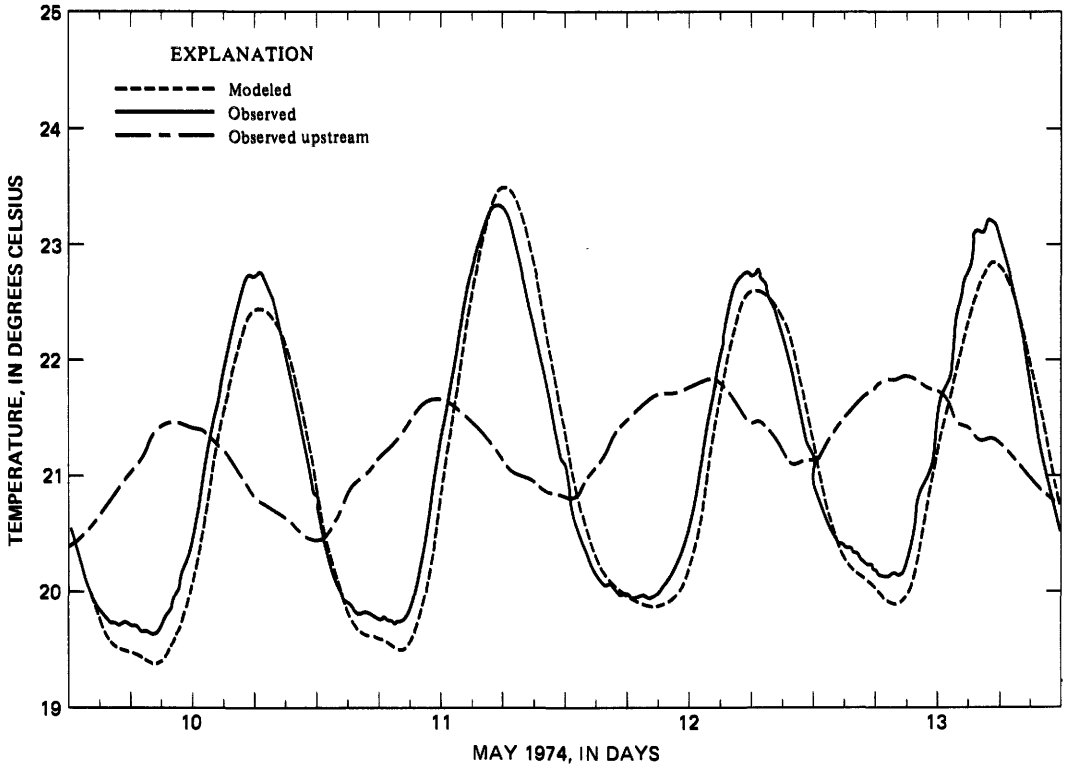

FIGURE 19.—Comparison of the modeled and observed temperatures at the downstream end of the San Diego Aqueduct during the first 4 days of the sixth verification.

on the San Diego Aqueduct in southern California. Analyzing the problem from both the Eulerian and Lagrangian point of view, it was possible to determine the two coefficients in a Dalton-type evaporation formula (eq. 21) by balancing the energy budget of the canal. The model was calibrated, that is, the coefficients were determined, using 28 days of data and verified with 113 different days of data.

During all seasons of the year, equation 21 appears to realistically represent the evaporation from the canal. Equation 21 is believed to be the first wind function ever derived from the thermal balance of an open channel. The derived wind function for the San Diego Aqueduct indicates a larger evaporation at low windspeeds than would be indicated by most lake evaporation formulas, but the mass-transfer coefficient is within the range of values commonly reported. An annual canal evaporation of 2.08 m is indicated; this figure is about 91 percent of the amount of water evaporated annually from nearby class A evaporation pans.

REFERENCES

Anderson, E. R., 1954, Energy budget studies, *in* Water-loss investigations: Lake Hefner studies, Technical Report: U.S. Geological Survey Professional Paper 269, p. 71–120.

Brown, G. W., 1969, Predicting temperatures of small streams: Water Resources Research, v. 5, no. 1, p. 68–75.

Carslaw, H. S., and Jaeger, J. C., 1959, Conduction of heat in solids (2d ed.): New York, Oxford University Press, p. 104.

Dingman, S. L. and Weeks, W. F., 1970, Temperature and ice distribution in the North Saskatchewan River below the Edmonton generating plant: Cold Regions Research and Engineering Laboratory, Hanover, N.H., Special Report 152, 31 p.

Fischer, Hugo B., 1973, Longitudinal dispersion and turbulent mixing in open channel flow: Annual Review of Fluid Mechanics, p. 59–78.

Fread, D. L., 1974, Numerical properties of implicit four-point finite difference equations on unsteady flow: National Oceanic and Atmospheric Administrative Technical Memorandum NWS HYDRO–18, 38 p.

Harbeck, G. E., Jr., 1962, A practical field technique for measuring reservoir evaporation utilizing mass-transfer theory: U.S. Geological Survey Professional Paper 272–E, p. E101–E105.

Jobson, Harvey E., 1973, The dissipation of excess heat from water systems: American Society of Civil Engineers, Journal of the Power Division, v. 99, no. P01, p. 89–103.

Jobson, Harvey E., and Sturrock, A. M., Jr., 1976, Comprehensive monitoring of meteorology, hydraulics and thermal regime of the San Diego Aqueduct, California: U.S. Geological Survey Open-File Report 76–628, 102 p.

Jobson, Harvey E. and Yotsukura, Nobuhiro, 1973, Mechanics of heat transfer in nonstratified open-channel flows, *in* Shen, Hsieh Wen, ed., Environmental impact on rivers (River mechanics III): Fort Collins, Colo., Hsieh Wen Shen, 67 p.

Jones, E. J., 1965, Temperature in California streams; part I, evaluation of thermograph records: U.S. Geological Survey open-file report, 31 p.

Koberg, Gordon, E., 1964, Methods to compute long-wave radiation from the atmosphere and reflected solar radiation from a water

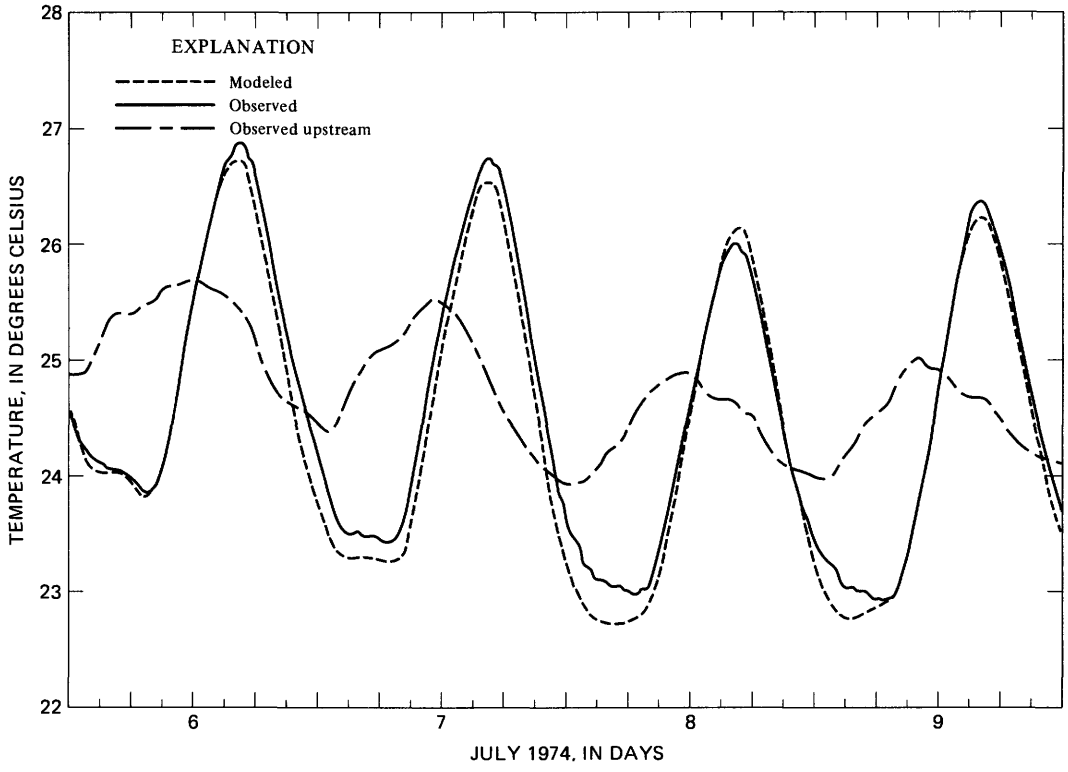

FIGURE 20.—Comparison of the modeled and observed temperatures at the downstream end of the San Diego Aqueduct during the first 4 days of the seventh verification.

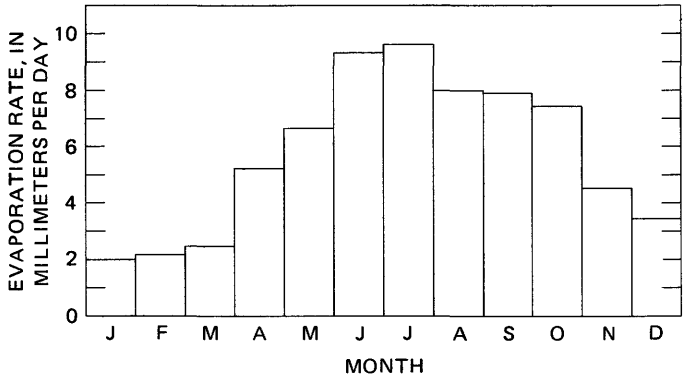

FIGURE 21.—Computed monthly average daily evaporation from the San Diego Aqueduct during the study period, July 25, 1973, to July 24, 1974.

surface: U.S. Geological Survey Professional Paper 272–F, p. F107–F136.

Kohler, M. A., Nordenson, T. J., and Baker, D. R., 1959, Evaporation maps of the United States: U.S. Weather Bureau Technical Paper 37, Washington, D.C., 13 p.

Linsley, R. K., Jr., Kohler, M. A., and Paulhus, J. L. H., 1958, Hydrology for engineers: New York, McGraw-Hill, 98 p.

Plukowski, E. J., 1970, Urbanization and its effect on the temperature of the streams on Long Island, New York: U.S. Geological Survey Professional Paper 627–D, 110 p.

Rawson, J., 1970, Reconnaissance of water temperature of selected streams in southeastern Texas: Texas Water Board, Austin, Tex., Report 105, 12 p.

Ryan, P. J., and Stolzenbach, K. D., 1972, Environmental heat transfer, *in* Engineering aspects of heat disposal from power generation: Mass. Institute of Technology, Cambridge, Ralph M. Parsons Laboratory for Water Resources and Hydrodynamics, summer session, 75 p.

Stone, H. L., and Brian, P. L. T., 1963, Numerical solution of convective transport problems: American Institute of Chemical Engineers Journal, v. 9, no. 5., p. 681–688.

Tennessee Valley Authority, 1972, Heat and mass transfer between a water surface and the atmosphere: Water Resources Research Laboratory Report 14, Norris, Tenn., 147 p.

Troxell, George Earl, and Davis, Harmer E., 1956, Composition and Properties of Concrete: New York, McGraw-Hill, 334 p.

Yotsukura, N. B., Fischer, H. B., and Sayre, W. W., 1970, Measurement of mixing characteristics of the Mississippi River between Sioux City, Iowa and Plattsmouth, Nebraska: U.S. Geological Survey Water-Supply Paper 1899–G, 29 p.